Electrochemistry Communications 179 (2025) 108033

Contents lists available at ScienceDirect

Electrochemistry Communications

journal homepage: www.elsevier.com/locate/elecom

Seven-parameter PEMFC model optimization using an battlefield optimization algorithm

Manish Kumar Singla [b,k,*], S.A. Muhammed Ali [a], Jyoti Gupta [d], Pradeep Jangir [e,f], Arpita [b], Ramesh Kumar [i], Reena Jangid [g,h], Mohammad Khishe [c,j,**]

[a] Fuel Cell Institute, Universiti Kebangsaan Malaysia, 43600 Bangi, Selangor, Malaysia
[b] Department of Biosciences, Saveetha School of Engineering, Saveetha Institute of Medical and Technical Sciences, Chennai 602 105, India
[c] Applied Science Research Centre, Applied Science Private University, 11937, Amman, Jordan
[d] School of Engineering and Technology, K. R. Mangalam University, Haryana, Gurgaon 122003, India
[e] Department of Electronics and Communication Engineering, Chandigarh University, Mohali 140413, India
[f] Innovation Center for Artificial Intelligence Applications, Yuan Ze University, Taoyuan 320315, Taiwan
[g] Department of CSE, Graphic Era Hill University, Dehradun 248002, Uttarakhand, India
[h] Department of CSE, Graphic Era Deemed To Be University, Dehradun 248002, Uttarakhand, India
[i] Department of Interdisciplinary Courses in Engineering, Chitkara University Institute of Engineering & Technology, Chitkara University, Punjab, India
[j] Department of Electrical Engineering, Imam Khomeini Naval Science University of Nowshahr, Nowshahr, Iran
[k] Jadara University Research Center, Jadara University, PO Box 733, Irbid, Jordan

ARTICLE INFO

Keywords:
Machine learning
Optimization
Fuel cell
Parameter estimation
Run time
Friedman ranking test

ABSTRACT

Precise modeling of Proton Exchange Membrane Fuel Cells (PEMFCs) requires accurate identification of key parameters, which are often unavailable from manufacturers but crucial for predicting fuel cell performance. The system relies on seven key parameters to determine activation and ohmic and concentration overpotential values through ξ1, ξ2, ξ3, ξ4, λ, Rc, and β. The Battlefield Optimization Algorithm (BfOA) represents a new optimization method that finds these seven essential PEMFC parameters effectively. Using Sum Squared Error (SSE) to minimize the difference between estimated and actual cell voltages, BfOA outperformed other optimization algorithms in determining parameters for six PEMFC models under varying operating conditions. The optimized parameters enabled accurate prediction of I-V and P—V curves, closely matching experimental data. BfOA's efficiency and robustness make it well-.

suited for real-time fuel cell modeling. Its effectiveness as a method for precise PEMFC device analysis within electronic component simulators is demonstrated. Future development will explore BfOA's compatibility with other fuel cell technologies, incorporate real-time data capabilities, and implement the algorithm in embedded systems for real-time PEMFC monitoring and control.

1. Introduction

Proton Exchange Membrane (PEM) fuel cells are key to a sustainable energy future, thanks to their high efficiency, quiet operation, and almost no emissions. These advantages make them very promising for commercial use, especially in transportation. However, their performance optimization is difficult due to the complex and non-linear relationships between design factors like activation overpotential, concentration overpotential, and internal resistance. Optimizing PEM fuel cell efficiency and reliability requires accurate modeling. While common optimization methods exist, they often struggle with these complex systems. They can be sensitive to initial values, get stuck in suboptimal solutions, and lack robustness when dealing with many interacting, non-linear variables. Therefore, developing specialized optimization algorithms for PEM fuel cells is crucial for wider adoption.

Research on PEM fuel cell modeling and optimization has yielded many advancements. Several studies have focused on parameter estimation using various optimization algorithms. For example, Kouache et al. used a self-adaptive bonobo optimizer for improved accuracy and efficiency, though they noted potential scalability issues [1]. El-Fergany

* Department of Biosciences, Saveetha School of Engineering, Saveetha Institute of Medical and Technical Sciences, Chennai 602 105, India
** Corresponding author at: Department of Electrical Engineering, Imam Khomeini Naval Science University of Nowshahr, Nowshahr, Iran.
E-mail addresses: msingla0509@gmail.com (M.K. Singla), mas@ukm.edu.my (S.A. Muhammed Ali), m_khishe@alumni.iust.ac.ir (M. Khishe).

https://doi.org/10.1016/j.elecom.2025.108033
Received 9 May 2025; Received in revised form 27 July 2025; Accepted 12 August 2025
Available online 16 August 2025

Table 1
Comprehensive analysis as per the previous studies.

References	Methodology	Key Findings	Limitations	Direct Applicability to Standard PEMFC Modeling
[25]	Improved Fish Migration Optimization	Potential for parameter identification.	Long term stability	Yes
[26]	Membrane Technologies	Explored water treatment applications	Directly applicable to PEMFCs.	Indirect
[27]	Neural	High accuracy in power and voltage prediction.	Model adaptability to different operating conditions.	Yes
[28]	Deep Reinforcement Learning	Promise in multi-system coordination for PEMFC control.	Computational limitations.	Yes
[29]	Modified Golden Jackal Optimization	Achieved improvements in parameter modeling.	Further real-world validation required.	Yes
[30]	Review of Machine Learning Applications	Comprehensive overview of ML for PEMFC optimization.	Practical implementation examples.	Yes
[31]	Bald Eagle Search Algorithm	Efficient PEMFC parameter identification	Performance under varying conditions.	Yes
[32]	Genetic Algorithms	Characterization of high-temperature PEMFCs.	Applicability to standard PEMFCs.	Limited (focused on high-temperature PEMFCs)
[33]	Neural Networks	Educational evaluation.	Relevance to PEMFC modeling.	NO
[34]	Multi-Objective Deep Reinforcement Learning	Promising results in PEMFC control.	Practical implementation examples.	Yes
[35]	Efficient, Accurate Parameter Estimation Algorithm	Proposed an efficient and accurate algorithm.	Scalability.	Yes
[36]	Improved Deterministic Policy Gradient Algorithm	Achieved good results in PEMFC control.	Adaptability.	Yes
[37]	Jellyfish Search Algorithm	Improvements in parameter extraction.	Scalability concerns.	Yes
[38]	Adaptive Sparrow Search Algorithm	Achieved accuracy in parameter identification.	Extensive experimental validation.	Yes
[39]	Robust SCCSA Optimization Algorithm	Developed a robust algorithm for parameter extraction.	Scalability.	Yes

et al. employed a Red-Billed Blue Magpie Optimizer to enhance electrical characterization, but lacked comparison with existing methods [2]. Saidi et al. used an enhanced salp swarm algorithm for robust parameter identification, but didn't include real-world validation [3]. Similarly, Elfar et al. developed a particle swarm optimization algorithm for effective performance optimization, but without extensive testing under different conditions [4]. Other PEMFC research has explored different optimization techniques. Yang et al. combined a neural network with a pelican optimization algorithm for faster and more accurate parameter identification, though scalability remained a question [5]. Shaheen et al. used a human memory optimizer, incorporating sensitivity and uncertainty analysis for robust modeling, but noted potential computational limitations for real-time use [6]. Sultan et al. developed a modified manta ray foraging optimization for more precise parameter identification, but didn't explore its applicability to different fuel cell types [7]. Houssein et al. introduced the Walrus Optimizer for parameter extraction, showing significant accuracy improvements, but without a thorough comparison to traditional methods [8].

More recent work includes Priya et al.'s use of the clan co-operative spotted hyena optimizer for PEMFC modeling, demonstrating computational efficiency but not thoroughly addressing parameter variability across different operating conditions [9]. Ashraf et al. surveyed AI-based techniques for solid oxide fuel cells, highlighting optimization gaps but focusing on a different fuel cell type, limiting its direct relevance to PEMFCs [10]. Zhang et al. achieved high accuracy with a swarm intelligence algorithm for PEMFC parameter identification, but didn't investigate computational scalability for large datasets [11]. Ebrahimi et al. used the Repairable Grey Wolf Optimization algorithm, achieving high accuracy in PEMFC parameter identification, but without experimental validation of their simulations [12]. Duan et al. used an amended deer hunting optimization algorithm for robust PEMFC parameter estimation, but without a detailed sensitivity analysis [13]. He et al. combined generalized regression neural networks with meta-heuristic algorithms for effective parameter identification, but noted potential computational limitations for real-time applications [14]. Rubio et al. explored distributed intelligence for autonomous PEM fuel cell control, achieving improved control system efficiency, but with limited discussion of scalability and adaptability [15].

Ali et al. used a coot bird optimizer for PEMFC models, demonstrating adaptability, but requiring practical validation [16]. Abdel-Basset et al. compared optimization methods, identifying promising approaches, but neglecting implementation issues [17]. Yang et al. reviewed mass transfer in PEMFCs, providing a strong theoretical basis, but lacking computational validation [18]. Guo et al. developed a digital twin for hybrid PV-SOFC systems, potentially relevant to PEMFCs, but focused on SOFCs [19]. Lastly, Mitra et al. reviewed PEMFC parameter estimation, highlighting methodological gaps, but not addressing real-world implementation challenges [20]. More recent research includes Liu et al.'s hybrid particle swarm optimization with differential evolution for PEMFC parameter identification, showing promise but raising concerns about computational cost for large-scale applications [21]. Abdel-Basset et al. evaluated improved metaheuristic algorithms for parameter selection, providing a detailed comparison, but lacking experimental validation [22]. Wang et al. proposed an improved chicken swarm optimization algorithm for parameter estimation, demonstrating potential, but lacking extensive validation against experimental data [23]. Rezk et al. used recent optimization algorithms, achieving high accuracy, but without a thorough scalability analysis [24].

Other studies have explored various approaches. Zhou et al. used an improved fish migration optimization for parameter identification, showing potential, but not addressing long-term stability [25]. Shalaby et al. explored membrane technologies for water treatment, which has some relevance to PEMFCs, but is not directly applicable [26]. Wilberforce et al. used neural networks for power and voltage prediction, achieving high accuracy, but not examining model adaptability to different operating conditions [27]. Li et al. implemented deep reinforcement learning for PEMFC control, showing promise in multi-system coordination, but noting computational limitations [28]. Rezaie et al. proposed a modified golden jackal optimization for parameter modeling, achieving improvements, but requiring further real-world validation [29]. Ding et al. reviewed machine learning applications for PEMFC optimization, providing a comprehensive overview, but without practical implementation examples [30]. Yang et al. used the Bald Eagle

Search Algorithm for efficient PEMFC parameter identification, but didn't explore its performance under varying conditions [31]. Losantos et al. used genetic algorithms for high-temperature PEMFC characterization, limiting its applicability to standard PEMFCs [32]. Liao used neural networks for educational evaluation, a topic with limited relevance to PEMFC modeling [33]. Li et al. applied multi-objective deep reinforcement learning for PEMFC control, achieving promising results, but lacking practical implementation examples [34]. In more recent work, Abdel-Basset et al. proposed an efficient, accurate parameter estimation algorithm, but without addressing scalability [35]. Li et al. used an improved deterministic policy gradient algorithm for PEMFC control, achieving good results, but not addressing adaptability [36]. Gouda et al. employed the Jellyfish Search Algorithm for parameter extraction, showing improvements, but raising scalability concerns [37]. Zhu et al. used the Adaptive Sparrow Search Algorithm for parameter identification, achieving accuracy, but lacking extensive experimental validation [38]. Alizadeh et al. developed a robust SCCSA optimization algorithm for parameter extraction, but without exploring scalability [39]. The Table 1 represents the comprehensive analysis as per the previous studies.

Despite significant progress in PEMFC modeling and optimization, several gaps remain. While much research focuses on developing new parameter identification and optimization algorithms (like swarm intelligence, evolutionary methods, and neural networks), scalability, real-world experimental validation, and computational efficiency under dynamic conditions remain challenging. Methods like the Red-Billed Blue Magpie Optimizer [2], manta ray foraging optimization [7], and hybrid particle swarm with differential evolution [21], while promising, often lack robustness for large-scale or real-time applications. Furthermore, advanced techniques like machine learning and digital twin modeling [19,30] are still under development and need better integration with traditional optimization. Finally, there's a lack of research on algorithms that can simultaneously handle conflicting objectives like accuracy, speed, and resource constraints. These gaps highlight the need for a new, hybrid optimization algorithm that combines the strengths of existing methods to provide a robust, efficient, and scalable solution for PEMFC parameter optimization, both theoretically and practically.

In this study, the Battlefield Optimization Algorithm (BfOA) [40] models a battle between two opposing forces, each employing potentially different strategies to achieve the same goal: victory. This concept mirrors the Marine Predators Algorithm (MPA), which also divides its population into two groups: predators and prey. BfOA is able to overcome the shortcomings of conventional and modern optimization algorithms by incorporating a novel combination of intensification and diversification strategies. Even for highly nonlinear PEMFC systems, it provides superior convergence speed and accuracy. These capabilities make BfOA a useful tool for advancing PEMFC technology and for optimizing its practical deployment in energy and transportation sectors. The main novelty of this research is the development and use of Battlefield Optimization Algorithm (BfOA) for the precise estimation of parameters of Proton Exchange Membrane Fuel Cells (PEMFCs). Unlike the traditional approach of optimization methods, BfOA brings in a novel dual-squad strategy based on military tactics to explore and exploit mechanisms to address the shortcomings of previous algorithms. The algorithm employs a Defense in Depth strategy for exploitative local search, and a Supit Urang formation for balanced exploration-exploitation, which allows fast exploration of complex, non-linear, PEMFC parameter spaces. The two-phase reconnaissance and battle strategy implemented by it guarantees strong convergence through avoidance of local optima which is a common problem in PEMFC modeling. BfOA outperforms the performance of nine state-of-the-art algorithms in twelve commercial PEMFC datasets in terms of lower Sum of Squared Errors (SSE), Absolute Error (AE), and Mean Bias Error (MBE). Moreover, it demonstrates greater convergence in 50 iterations and reduced computational runtime, thus, making it very appropriate for real time applications. Confirmed through a variety of operating conditions, i.e. changes in temperature, pressure, and current density, BfOA is always superior over former methods in determining I-V and P—V characteristics with little deviation from experimental data. This adaptability is further confirmed by the superior performance in best-ranking Friedman statistical test for large scale and dynamic systems increasing its robustness. In addition to PEMFCs, the battlefield-inspired mechanics of BfOA provide a transferable paradigm for optimizing other energy-systems and non-linear engineering problems. This research closes a crucial gap in PEMFC modeling by presenting a very accurate, computationally fast and universal optimization tool, a major improvement in fuel cell parameter estimation.

The main novelty of this research is the development and use of Battlefield Optimization Algorithm (BfOA) for the precise estimation of parameters of Proton Exchange Membrane Fuel Cells (PEMFCs). Unlike the traditional approach of optimization methods, BfOA brings in a novel dual-squad strategy based on military tactics to explore and exploit mechanisms to address the shortcomings of previous algorithms. The algorithm employs a Defense in Depth strategy for exploitative local search, and a Supit Urang formation for balanced exploration-exploitation, which allows fast exploration of complex, non-linear, PEMFC parameter spaces. The two-phase reconnaissance and battle strategy implemented by it guarantees strong convergence through avoidance of local optima which is a common problem in PEMFC modeling. BfOA outperforms the performance of nine state-of-the-art algorithms in twelve commercial PEMFC datasets in terms of lower Sum of Squared Errors (SSE), Absolute Error (AE), and Mean Bias Error (MBE). This adaptability is further confirmed by the superior performance in best-ranking Friedman statistical test for large scale and dynamic systems increasing its robustness. In addition to PEMFCs, the battlefield-inspired mechanics of BfOA provide a transferable paradigm for optimizing other energy-systems and non-linear engineering problems. This research closes a crucial gap in PEMFC modeling by presenting a very accurate, computationally fast and universal optimization tool, a major improvement in fuel cell parameter estimation.

The contributions of this research are summarized as follows:

- Application to PEMFCs: The BfOA algorithm is applied to optimize design variables for twelve PEMFC sheets: BCS 500 W [41] [42], SR-12500 W [41,42], STD 250 W [41] [42], Nedstack 600 W PS6 [43], Horizon H-12 [44], and Ballard Mark V [44].
- Comparative Analysis: The performance of BfOA is benchmarked against nine state-of-the-art algorithms, including Thermal Exchange Optimization (TEO) [45], Grey Wolf optimization (GWO) [46], Rime Optimization (RIME) [47], Equilibrium Optimizer (EO) [48], Marine Predators Algorithm (MPA) [49], Komodo Mlipir Algorithm (KMA) [50], Self-Adaptive Differential Evolution (SaDE) [51], White Shark Optimizer (WSO) [52], and Genetic Algorithm (GA) [53], across a range of optimization scenarios.
- Environmental Impact Assessment: The impact of varying temperature and pressure conditions on PEMFC performance is evaluated, demonstrating the adaptability and reliability of the optimized models.
- The proposed algorithm demonstrates superior performance through its achievement of reduced sum of squared errors (SSE) and absolute error (AE) and relative error (RE) and mean bias error (MBE) when compared to traditional algorithms. Additionally it requires less computational time. BfOA achieves faster computational processing which makes it appropriate for real-time PEMFC parameter optimization tasks.
- Scalability and Efficiency: Demonstrating the scalability of BfOA across multiple PEMFC configurations, ensuring its adaptability to varying operational scenarios and design constraints.

This paper is structured as follows: Section 2 details the PEMFC mathematical model, including design variables and optimization objectives. Section 3 introduces the Battlefield Optimization algorithm,

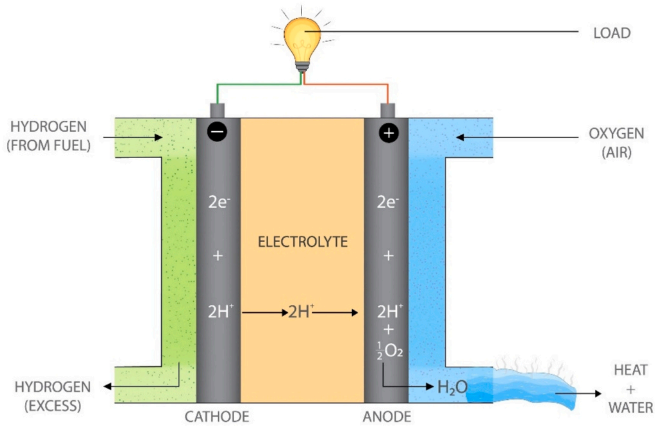

Fig. 1. Schematic Diagram of PEMFC.

explaining its features and implementation. Section 4 presents simulation results and a comparison with other algorithms. Section 5 concludes the paper, summarizing contributions and outlining future research directions.

2. PEMFC mathematical modeling

2.1. Basic concept of PEMFCs

The core structure of a Proton Exchange Membrane Fuel Cell (PEMFC) consists of two electrodes the anode and the cathode separated by a proton-conducting membrane, which serves as the polymer electrolyte. A schematic representation of this fuel cell is provided in Fig. 1.

A specific design allows protons to move through it, but blocks electrons [54]. To speed up the reaction, catalyst layers are positioned between the electrolyte membrane and both electrodes. In this process, hydrogen gas enters the anode and, upon reaching the catalyst layer, dissociates into protons and electrons. The protons pass through the electrolyte membrane to the cathode's catalyst layer, while the electrons travel through an external circuit. Simultaneously, oxygen or air is supplied to the cathode. When oxygen reaches the cathode's catalyst layer, it reacts with the protons from the membrane and the electrons from the external circuit, forming water. The electrochemical reactions occurring at the PEMFC electrodes are represented as follows [54]:

Anode reaction

$$H_2 \rightarrow 2H^+ + 2e^- \# \tag{1}$$

Cathode reaction

$$2H^+ + \frac{1}{2}O_2 \rightarrow H_2O \# \tag{2}$$

Overall reaction:

$$H_2 + \frac{1}{2}O_2 \rightarrow H_2O + \text{Energy} + \text{Heat} \# \tag{3}$$

In Eq. (3), the term "Energy" represents the electrical energy generated as a result of electron flow from hydrogen gas traveling from the anode to the cathode through an external load.

2.2. Mathematical model of PEMFC

The output voltage V_{cell} of each individual fuel cell can be computed using the following expression [55,56]:

$$V_{\text{cell}} = E_{\text{nerst}} - \Delta V_{\text{act}} - \Delta V_{\text{ohm}} - \Delta V_{\text{con}} \# \tag{4}$$

In this equation, E_{nerst} denotes the open-circuit voltage of the cell, ΔV_{act} represents the activation overpotential per cell, ΔV_{ohm} describes the voltage drop caused by ohmic resistance due to electron conduction through the external load and the proton movement resistance in the electrolyte membrane, and ΔV_{con} indicates the concentration overpotential per cell. Amphlett et al. [57] proposed a model of a fuel cell electrochemical properties. When a series connection of N_{cells} identical fuel cells is configured for increased voltage output, the total stack voltage can be determined as:

$$V_{\text{stack}} = N_{\text{cells}} \cdot V_{\text{cell}} \# \tag{5}$$

Here, N_{cells} refers to the number of cells connected in series, and V_{cell} is the output voltage for each individual fuel cell, as derived from Eq. (4).

The reversible potential, E_{nerst}, is calculated as follows [58,59]:

$$E_{nerst} = 1.229 - 8.5 \times 10^{-4}(T_{\text{fc}} - 298.15) + 4.3085 \times 10^{-5} T_{\text{fc}} \cdot \left[\ln(P_{H_2}) + \ln\left(\sqrt{P_{O_2}}\right)\right] \# \tag{6}$$

where T_{fc} is the cell absolute operating temperature in Kelvin, while P_{H_2} and P_{O_2} denote the partial pressures of hydrogen and oxygen in the fuel cell stack input channels (atm). When hydrogen and air serve as the inputs, the partial oxygen pressure, P_{O_2}, is determined as follows [60,61]:

$$P_{O_2} = P_{\text{c}} - RH_{\text{c}} P_{H_2O}^{\text{sat}} - \frac{0.79}{0.21} P_{O_2} \cdot \exp\left(0.291 \frac{I_{\text{fc}}}{A} \Big/ T_{\text{fc}}^{0.832}\right) \# \tag{7}$$

where P_{c} represents the inlet channel pressure at the cathode (atm), RH_{c} is the cathode electrode relative humidity, I_{fc} is the operating current (A), A is the membrane surface area (cm^2), and $P_{H_2O}^{\text{sat}}$ is the water vapor pressure at saturation, defined by [62]:

$$\log_{10}\left(P_{H_2O}^{\text{sat}}\right) = 2.95 \times 10^{-2}(T_{\text{fc}} - 273.15) - 9.18 \times 10^{-5}(T_{\text{fc}} - 273.15)^2 + 1.44 \times 10^{-7}(T_{\text{fc}} - 273.15)^3 - 2.18 \# \tag{8}$$

In cases where hydrogen and pure oxygen are used, the partial oxygen pressure P_{O_2} is calculated as follows [62]:

$$P_{O_2} = RH_{\text{c}} P_{H_2O}^{\text{sat}} \left[\left(\exp\left(4.192 \frac{1}{I_{\text{fc}}} \Big/ T_{\text{fc}}^{1.334}\right) \frac{RH_{\text{c}} P_{H_2O}^{\text{sat}}}{P_{\text{a}}}\right)^{-1} - 1\right] \# \tag{9}$$

In both cases, the partial hydrogen pressure P_{H_2} is given by:

$$P_{H_2} = 0.5 RH_{\text{a}} P_{H_2O}^{\text{sat}} \left[\left(\exp\left(1.635 \frac{1}{I_{\text{fc}}} \Big/ T_{\text{fc}}^{1.334}\right) \cdot \frac{RH_{\text{a}} P_{H_2O}^{\text{sat}}}{P_{\text{a}}}\right)^{-1} - 1\right] \# \tag{10}$$

where P_{a} is the anode electrode inlet channel pressure (atm), and RH_{a} indicates the relative humidity on the anode side.

The activation voltage drop ΔV_{act} for the electrodes is calculated by:

$$\Delta V_{\text{act}} = -\left[\xi_1 + \xi_2 T_{\text{fc}} + \xi_3 T_{\text{fc}} \ln(C_{O_2}) + \xi_4 T_{\text{fc}} \ln(I_{\text{fc}})\right] \# \tag{11}$$

where ξ_1, ξ_2, ξ_3, and ξ_4 are empirical coefficients, and C_{O_2} denotes the oxygen concentration at the cathode (mol/cm^3) as follows:

$$C_{O_2} = \frac{P_{O_2}}{5.08 \times 10^6 \cdot \exp\left(-498 \big/ f_{\text{fc}}\right)} \# \tag{12}$$

The ohmic resistive voltage drop ΔV_{ohm} is determined by:

$$\Delta V_{\text{ohm}} = I_{\text{fc}}(R_M + R_C) \# \tag{13}$$

where R_M is the membrane resistance (Ω) and R_C is the resistance due to proton movement through the membrane. Membrane resistance is calculated as:

$$R_M = \frac{\rho_M \cdot l}{A} \# \tag{14}$$

with ρ_M being specific membrane resistance (Ω·cm), l representing membrane thickness (cm), and the empirical formula for ρ_M given as:

$$\rho_M = \frac{181.6\left[1 + 0.03\left(\frac{I_{fc}}{A}\right) + 0.062\left(\frac{T_{fc}}{303}\right)^2\left(\frac{I_{fc}}{A}\right)^{2.5}\right]}{\left[\lambda - 0.634 - 3\left(\frac{I_{fc}}{A}\right)\right] \times \exp\left[4.18\left(\frac{T_{fc}-303}{T_{fc}}\right)\right]} \tag{15}$$

where λ is an adjustable parameter connected to membrane preparation.

The concentration voltage drop, ΔV_{con}, is determined by:

$$\Delta V_{\text{con}} = -b\ln\left(1 - \frac{J}{J_{\max}}\right) \tag{16}$$

where b is a parametric coefficient (V); J and $J_{\max}$ are the current density and maximum current density (A/cm^2), respectively.

To ensure accurate modeling under simulation and control conditions, precise estimation of these parameters is essential. Seven unknown parameters ($\xi_1, \xi_2, \xi_3, \xi_4, \lambda, R_C$, and b) are optimized using the proposed optimization technique.

2.3. Objective function

To ensure the model's results closely match real-world PEMFC experiments, researchers used an optimization method. This method works by reducing the difference between the model's voltage predictions and the voltages measured in experiments [63,64]. Specifically, they minimized the sum of squared errors (SSE) between these two sets of voltage values.

$$\text{OF} = \min\text{SSE}(x) = \min\sum_{i=1}^{N}\left[v_{\text{meas}}(i) - v_{\text{cal}}(i)\right]^2\# \tag{17}$$

where x represents the unknown parameter vector, N is the number of data points, i is the iteration index, v_{meas} is the measured PEMFC voltage, and v_{cal} is the estimated voltage. The optimization is subject to the following constraints:

$$\begin{array}{c} \xi_{i,\min} \le \xi_i \le \xi_{i,\max}, i = 1:4 \\ \hline R_{C\min} \le R_C \le R_{C\max} \\ \lambda_{\min} \le \lambda \le \lambda_{\max} \\ b_{\min} \le b \le b_{\max} \end{array} \tag{18}$$

where $\xi_{i,\min}$ and $\xi_{i,\max}$ are the limits for empirical coefficients, $R_{C,\min}$ and $R_{C,\max}$ are resistance bounds, and $\lambda_{\min}$, $\lambda_{\max}$, $b_{\min}$, and $b_{\max}$ define the limits for water content and parametric coefficients. The mean bias error for voltage is calculated as per below equation:

$$MBE = \frac{\sum_{i=1}^{N}\left|V_{meas}(i) - V_{calc}(i)\right|}{N} \tag{19}$$

3. Battlefield optimization algorithm (BfOA)

The Battlefield Optimization Algorithm (BfOA) is an optimization method that simulates a battle between two opposing forces with different strategies aiming for victory. It divides the population into two squads: a stronger (higher fitness) defending squad that exploits the promising region around its position, and a weaker attacking squad that moves towards the defender to improve its fitness while also exploring locally to avoid local optima. BfOA's battle phase emphasizes exploitation of promising regions identified in an initial exploration phase.

Phase 1: Deployment of Squad:

Sun Tzu's [65] emphasis on strategic positioning in "The Art of War" highlights the advantage conferred by a strong starting point. BfOA leverages the concept of reconnaissance aircraft to achieve this, using them to explore the search space and identify promising regions likely to contain the global optimum. Just as in real-world warfare, where aircraft serve various roles including bombing, support, and reconnaissance [66], BfOA's aircraft prioritize exploration. Their speed makes detailed exploitation difficult, resulting in a highly explorative first phase of the algorithm. Each squad in BfOA employs eight aircraft for reconnaissance, not to pinpoint the global optimum itself, but rather to identify promising surrounding regions. This strategy aims to strategically position the squads, avoiding entrapment in local optima. The aircraft are deployed to four distinct areas to maximize coverage of the search space. After a set number of iterations, the reconnaissance phase concludes, and the best positions identified by the aircraft are used to initialize the squads for the algorithm's second phase: the battle.

Phase 2: Battle:

Phase two of BfOA simulates a battle where the two squads adopt distinct tactics. The squad occupying the superior position (higher fitness value) assumes a defensive posture, while the other attacks. Mirroring Clausewitz's observation in "On War" (Friedman, 2017) [67] that "Defense has a passive purpose: preservation; and attack a positing one: conquest," the defending squad aims to maintain its positional advantage, while the attacking squad strives to capture it. The defending squad in BfOA employs a "Defense in Depth" tactic, establishing layers of fortifications to resist the attacker. This fort construction is a highly exploitative process, as squad members meticulously search their immediate vicinity for optimal positions. Meanwhile, the attacking squad utilizes a "Supit Urang" formation, characterized by a highly exploitative core and moderately explorative flanks.

Step 1: Squad Defending: The "Defense in Depth" tactic, employed by the defending squad, is a strategy used not only in military contexts but also in fields like IT and network security [68]. Its key advantage lies in its multi-layered approach. Rather than relying on a single, strong defensive line, Defense in Depth establishes multiple lines of defense, each activated as the preceding one is breached. In BfOA, these lines are created by layering fortifications. The defending squad in BfOA primarily focuses on exploiting the area around its current location. Within this squad, individual members act as builders, tasked with constructing fortifications at varying distances from the commander's position.

Step 2: Squad Attacking: The attacking squad in BfOA needs a strategy that balances exploitation with a moderate degree of exploration, allowing it to seek alternatives if it encounters a local optimum. The "Supit Urang" (Crab Claw) formation, a traditional Indonesian battle tactic, is well-suited to this purpose. While its precise origins are unclear, "Supit Urang" appears in numerous Indonesian historical fiction works, including *Senopati Pamungkas* [69] and *Gajah Mada* [70], as well as many stories by S.H. Mintardja. Notably, this formation was effectively used by General Soedirman during Indonesia's war of independence, contributing to his guerilla warfare successes [71]. Within BfOA's attacking "Supit Urang" formation, the core squad focuses on exploitation, advancing directly towards the defending squad's commander (the current best-fit position). The flanking squads, composed of cavalry (mirroring their historical role in flanking maneuvers [72]), perform a moderate level of exploration, moving perpendicularly to the core's direction. The core squad itself comprises the commander and a special forces soldier. Intriguingly, the attacking squad's builders mimic the defending squad's builders, constructing (ostensibly) fortifications, but at different ranges. This tactic deepens the exploitation of the defending squad's position.

3.1. BfOA mathematical model

Step 1: Best Fitness Criteria: Unlike many optimization algorithms that only replace a current solution with a new one if the new solution has a superior fitness value, BfOA takes a different approach. BfOA only rejects a new solution if its fitness value is worse than the current one. This strategy is designed to address the challenge of flat search spaces. In such regions, a solution might become trapped because neighboring positions have identical fitness values, preventing movement. By accepting a new solution, even if it has the same fitness, BfOA encourages movement, potentially leading the solution out of the flat area and closer to a region with varying fitness values. The decision-making process in BfOA can be summarized as in Eq. 20:

$$pos_{i+1} = \begin{cases} pos_i, if\ f(pos_i) < f(pos_{i+1}) \\ pos_{i+1}, otherwise \end{cases} \tag{20}$$

Step 2: First Phase: Each squad utilizes eight aircraft to explore the search space, aiming to identify optimal deployment locations. This reconnaissance is intended to position the squads within the region of the global optimum, avoiding entrapment in local optima. Numerous movement models exist for simulating the aircraft's search patterns. Other algorithms have employed Random Walks [73], Levy Flight [74], or Brownian Motion [75]. Research by [48] suggests that Brownian Motion, due to its broader search pattern compared to Levy Flight, is particularly well-suited for the reconnaissance flights in BfOA. The aircraft movement is defined by Eq. 21.

$$apl_{i+1} = apl_i + apl_{i \bullet \sigma r_\sigma} \tag{21}$$

In this equation, σ represents the standard deviation of displacement, and $r\sigma$ is a normally distributed random number. The magnitude of σ controls the extent of the aircraft's movement. A large σ value is unsuitable for small search areas, as it would likely cause the aircraft to stray outside the boundaries. Conversely, a small σ value in a large search area would restrict exploration, reducing the chance of locating the global optimum. BfOA categorizes search areas by length: small (less than 20), medium (20−100), and large (greater than 100), and assigns a unique σ value to each category.

Step 3: Commander: The commander leads each squad and is initially assigned the squad's best-known position (highest fitness value) at the start of each iteration. A comparison of the commanders' fitness values determines which squad will defend and which will attack. The squad with the higher fitness value defends, while the other attacks. During an attack, the commander leads the exploitation process by moving towards the opposing commander's position (the best fitness value found by the enemy squad), as implemented in Eq. 22. When defending, the commander transitions into a builder, constructing an additional fortification.

$$cmd_{i+1} = cmd_i + \frac{enemy_i - cmd_i}{norm(enemy_i - cmd_i)} \bullet r_{cmd} \bullet const_{cmd} \tag{22}$$

In this equation, $enemy_i$ represents the position of the opposing squad's commander, r_{cmd} is a random number drawn from a uniform distribution between 0 and 1, and $const_{cmd}$ is a constant that influences the commander's movement distance.

Step 4: Special Force: Special Forces are elite military units, sometimes referred to as Special Operations forces, due to the unique nature of their missions [76]. These units are typically composed of highly skilled personnel selected for their superior abilities. They undertake complex and challenging missions. The United States Navy SEALs, known for their successful operation to eliminate Al Qaeda leader Osama bin Laden [77], serve as a prime example of a Special Forces unit. In BfOA, the Special Forces unit is tasked with rapid attacks, aiming to reach the optimum position as quickly as possible. Their movement is directed towards a specific target, determined by the optimization goal: higher values for maximization problems and lower values for minimization problems. This directed movement is highly exploitative, accelerating the squad's progress towards the optimum. However, this speed carries the risk of incorrect directional movement, potentially leading to ineffective searches. Despite this risk, the potential benefits outweigh the drawbacks, as the Special Forces' movement does not negatively impact the other squad members. The Special Forces' movement is defined by Eq. 23.

$$spf_{i+1} = (1 + r_{spf}) \bullet spf_i \bullet const_{spf} \tag{23}$$

In this equation, r_{spf} represents a random number drawn from a uniform distribution, and $const_{spf}$ is a constant that influences the Special Force's movement.

Step 5: Cavalry: Cavalry units are known for their speed and maneuverability, historically used for screening infantry, flanking maneuvers, and pursuing retreating enemies. In BfOA, cavalry units execute the flanking maneuvers within the attacking "Supit Urang" formation. Their movement is perpendicular to the enemy commander's position with one cavalry unit moving left and the other right. This movement pattern deviates from direct exploitation of the best-known position (the enemy commander's location). Instead, the cavalry explore alternative directions, seeking escape routes should the squads become trapped in a local optimum. The equations governing the left and right cavalry movements are shown in Eq. 24 and Eq. 25.

$$cavl_{i+1} = (cavl_i - v_{perp}) \bullet const_{cav} \tag{24}$$

$$cavr_{i+1} = (cavr_i - v_{perp}) \bullet const_{cav} \tag{25}$$

In these equations, v_{perp} represents a perpendicular vector with a random distance between the cavalry unit and the enemy commander's position, and $const_{cav}$ is a constant influencing the cavalry's movement.

Step 6: Builders: Builders are integral to the defending squad. When a squad adopts a defensive posture, all members transition into builders, constructing layered fortifications. During an attack, a subset of the attacking squad also functions as builders. All builders, regardless of which squad they belong to, construct fortifications within a defined perimeter around the defending squad's commander. Deploying multiple builders across varying ranges increases the likelihood of successful exploitation and improves the chances of discovering hidden valleys within the search space. Builder movement in BfOA is defined as shown in Eq. 26:

$$bld_{i+1} = bld_i - coeff \bullet v_{bld} \tag{26}$$

In this equation, *coeff* is a random number between −1 and 1, and v_{bld} is a constant for the builder's movement. This builder constant is dynamically adjusted during the optimization process. Initially set to 1E-1, 1E-2, 1E-3 for the three builders respectively, it is reduced by a factor of 10 every 50 iterations until the third builder's constant reaches 1E-8. At this point, the builder constants are reset to their initial values. This dynamic adjustment facilitates the construction of layered fortifications. In contrast, the movement constants for commanders and cavalry remain fixed throughout the optimization process at 1E-1 and 1E-3, respectively. The Algorithm 1 shows the pseudocode of battlefield optimization algorithm.

Algorithm 1 Pseudo Code of Battlefield Optimization Algorithm

```
Result: P_best as the global optimum solution
Set n as the number of phase 1 function evaluation;
Initialization of 16 individuals with m dimensions in four areas;
Assign the individuals of areas 1 and II to air squad 1;
Assign the individuals of areas III and IV to air squad 2;
While number of Function Evaluation < n && Stopping Criterion = false do
Move all airplanes using Eq. (21);
Calculate the quality of all airplanes;
If quality (best airplane) >= quality (best history) then
Replace best history with best airplane;
End
End
Assign 7 best individuals of each air squad to the squad;
While Stopping Criterion = false do
If quality (commander 1) > quality (commander 2) then
Move commander 1 using Eq. (26);
Move left cavalry 1 using Eq. (26);
Move right cavalry 1 using Eq. (26);
Move builders 1 using Eq. (26);
Move commander 2 using Eq. (22);
Move left cavalry 2 using Eq. (24);
Move right cavalry 2 using Eq. (25);
Move builders 2 using Eq. (26);
End
If quality (commander 2) > quality (commander 1) then
Move commander 1 using Eq. (22);
Move left cavalry 1 using Eq. (24);
Move right cavalry 1 using Eq. (25);
Move builders 1 using Eq. (26);
Move commander 2 using Eq. (26);
Move left cavalry 2 using Eq. (26);
Move right cavalry 2 using Eq. (26);
Move builders 2 using Eq. (26);
End
Move special force 1 and 2 using Eq. (26);
Rank each squad member and reassign according to the rank;
Select the highest quality troops as P_best;
End
```

4. Results and discussion

Twelve different PEMFC sheets (BCS 500 W, Nedstack 600 W PS6, SR-12 W, Horizon H-12, Ballard Mark V, and STD 250 W) were optimized using both experimental and computational methods. Experiments utilized manufacturer-provided voltage-current data, supplemented by real-time gas pressure and cell temperature measurements obtained with digital multimeters, pressure sensors, and thermocouples (specifications in Table 2). Computational optimization employed the Battlefield Optimization Algorithm (BfOA), a phased search algorithm, to minimize the sum of squared errors (SSE) between measured and modeled voltage. BfOA's performance was compared

Table 2
Twelves PEMFCs Manufacturer sheets.

S.NO	SHEET 1	SHEET 2	SHEET 3	SHEET 4	SHEET 5	SHEET 6	SHEET 7	SHEET 8	SHEET 9	SHEET 10	SHEET 11	SHEET 12
PEMFC Type	BCS 500 W	NetStack PS6	SR-12	H-12-1	Ballard Mark V	STD -1	Horizon	STD -2	STD -3	STD -4	H-12-2	H-12-3
Power(W)	500	6000	500	12	5000	250	500	250	250	250	12	13
Ncells (no)	32	65	48	13	35	24	36	24	24	24	13	13
A(cm^2)	64	240	62.5	8.1	232	27	52	27	27	27	8.1	8.1
l(um)	178	178	25	25	178	127	25	127	127	127	25	25
T(K)	333	343	323	323	343	343	338	343	343	343	302	312
Jmax(mA/cm^2)	469	1125	672	246.9	1500	860	446	860	860	860	246.9	246.9
PH_2(bar)	1.0	1.0	1.47628	0.4935	1.0	1.0	0.55	1.5	2.5	2.5	0.4	0.5
PO_2(bar)	0.2095	1.0	0.2095	1.0	1.0	1.0	1.0	1.5	3.0	3.0	1.0	1.0

Table 3
Parameter Optimization and Function Maximization for Sheet 1.

Algorithm	GWO	EO	MPA	KMA	SaDE	WSO	RIME	TEO	GA	BfOA
ξ_1	−1.04619	−1.16703	−1.19969	−0.93049	−1.09529	−1.04499	−1.01161	−1.17951	−0.8532	−0.85805
ξ_2	0.003726	0.003829	0.003378	0.002427	0.003001	0.002796	0.003612	0.003799	0.002213	0.002611
ξ_3	0.000098	8.15E-05	4.61E-05	3.69E-05	4.21E-05	3.86E-05	9.75E-05	7.71E-05	3.84E-05	6.28E-05
ξ_4	−0.00019	−0.00019	−0.00019	−0.00019	−0.00019	−0.00019	−0.00019	−0.00019	−0.00019	−0.00019
λ	21.73713	22.99929	20.8771	21.28904	20.88524	21.67374	20.75523	20.95835	20.35153	20.87724
R_c	0.00057	0.000316	0.0001	0.00011	0.000117	0.00012	0.000109	0.000106	0.0001	0.0001
B	0.013737	0.016132	0.016126	0.016284	0.016069	0.016694	0.01603	0.016139	0.015027	0.016126
Min.	0.039303	0.025757	0.025493	0.025684	0.025531	0.026438	0.025543	0.025499	0.040688	0.025493
Max.	0.316639	0.040186	0.107157	0.035608	0.027295	0.051654	0.026825	0.025606	0.300867	0.025566
Mean	0.111066	0.031229	0.036852	0.029503	0.026123	0.033098	0.025879	0.025524	0.11969	0.025498
Std.	0.061157	0.004856	0.018237	0.002945	0.000645	0.006238	0.00029	3.24E-05	0.070558	1.8E-05
RT	12.67323	13.57184	11.1359	11.59972	23.07784	13.44444	12.35736	14.84043	24.45929	0.480288
FR	9.473684	6.368421	6.105263	5.842105	4.052632	6.736842	3.789474	2.052632	9.473684	1.105263

Table 4
Performance metrics of the Proposed algorithm for Sheet 1.

Vcell	Icell	Vest	AE	Pest	Pref	MBE	RE %
29	0.6	28.99722	0.002777	17.39833	17.4	4.28E-07	0.009575
26.31	2.1	26.30594	0.004063	55.24247	55.251	9.17E-07	0.015443
25.09	3.58	25.09356	0.003555	89.83493	89.8222	7.02E-07	0.01417
24.25	5.08	24.25462	0.00462	123.2135	123.19	1.19E-06	0.019053
23.37	7.17	23.37542	0.005416	167.6017	167.5629	1.63E-06	0.023175
22.57	9.55	22.58461	0.014615	215.6831	215.5435	1.19E-05	0.064754
22.06	11.35	22.07133	0.011327	250.5096	250.381	7.13E-06	0.051348
21.75	12.54	21.75846	0.008463	272.8511	272.745	3.98E-06	0.038913
21.45	13.73	21.46126	0.011263	294.6631	294.5085	7.05E-06	0.052506
21.09	15.73	20.98774	0.102258	330.1372	331.7457	0.000581	0.484867
20.68	17.02	20.69451	0.014509	352.2206	351.9736	1.17E-05	0.070162
20.22	19.11	20.23099	0.010986	386.6141	386.4042	6.71E-06	0.054332
19.76	21.2	19.77094	0.010943	419.144	418.912	6.65E-06	0.055381
19.36	23	19.36602	0.006025	445.4186	445.28	2.02E-06	0.03112
18.86	25.08	18.86647	0.006466	473.171	473.0088	2.32E-06	0.034286
18.27	27.17	18.27472	0.004721	496.5242	496.3959	1.24E-06	0.025838
17.95	28.06	17.95331	0.003311	503.7699	503.677	6.09E-07	0.018444
17.3	29.26	17.29288	0.007123	505.9896	506.198	2.82E-06	0.041174
			0.012913			**3.61E-05**	**0.061363**

against nine other advanced optimization algorithms (GWO, EO, MPA, KMA, SaDE, WSO, RIME, TEO, and GA). All simulations were run in MATLAB R2023a with a population size of 40 and a maximum of 500 iterations.

A thorough examination of the Battlefield Optimization Algorithm (BfOA) required the selection of nine state of the art optimization algorithms for comparison based on their unique characteristics, popularity, and applicability to PEMFC parameter estimation. The selected algorithms are a reflection of various optimization paradigms, such as swarm intelligence, evolutionary computation and physics inspired methods, thus providing a robust benchmarking framework. Grey Wolf Optimizer (GWO) [46] A swarm-based metaheuristic based on the hierarchical hunting behavior of grey wolves. GWO is well known for the balance between exploration and exploitation, which makes it appropriate for nonlinear optimization problems. Equilibrium Optimizer (EO) [48] A physics-inspired algorithm that is based on dynamic mass balance models. EO is good in escaping local optima because of its equilibrium based search mechanism. Marine Predators Algorithm (MPA) [49] A bio-inspired optimizer that models predator-prey dynamics in marine ecosystems. MPA is chosen because of its adaptive transition between exploration and exploitation phases. Komodo Mlipir Algorithm (KMA) [50] A new nature-inspired algorithm, which imitates the hunting behavior of Komodo dragons. KMA exhibits high convergence properties in high dimensional spaces. Self-Adaptive Differential Evolution (SaDE) [51] An evolutionary algorithm with parameters that are adaptive. SaDE is selected due to its ability to cope with multimodal and non-differentiable objective functions. White Shark Optimizer (WSO) [52] A metaheuristic that is based on the foraging behavior of white sharks. WSO is outstanding in global search capabilities and is applicable for engineering optimization tasks. Rime Optimization (RIME) [47] A physics based algorithm based on the rime-ice phenomenon. RIME is known to have good local search and no premature convergence. Thermal Exchange Optimization (TEO) [45] An algorithm based on thermodynamics that describes heat exchange between objects. TEO is applicable for constrained and unconstrained optimization. Genetic Algorithm (GA) [53] A traditional evolutionary algorithm used as a benchmark for comparison. GA's population based stochastic search serves as a benchmark for convergence behavior. The choice of these algorithms guarantees that the comparison is balanced across various optimization strategies such as exploration-exploitation trade-offs, convergence speed and accuracy of solutions. Their performance is critically assessed through the use of statistical metrics (SSE, MBE, RE) and computational efficiency (runtime), which shows the superiority of BfOA in PEMFC parameter estimation.

SHEET 1:

The BfOA excelled in optimizing the Sheet 1 PEMFC, providing accurate parameter estimates, fast convergence, and consistent results. Table 3 shows BfOA achieving the lowest mean (0.025498) and minimum (0.025493) SSE, surpassing both traditional algorithms like GA (0.11969) and GWO (0.111066), and newer ones like TEO (0.025524)

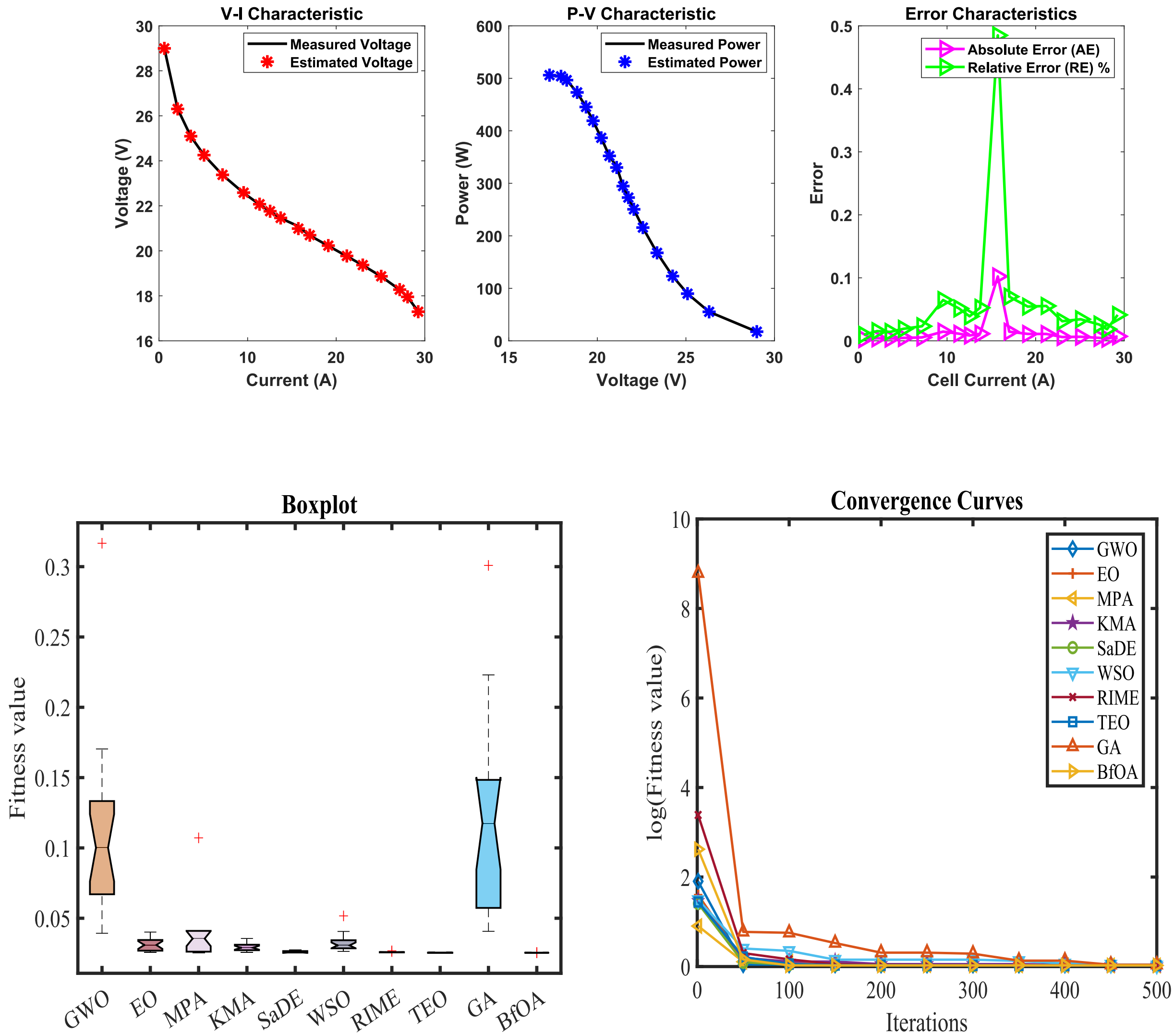

Fig. 2. Characteristic curves (a) P—V, V—I, and Error Curve, (b) Box-Plot (c) Convergence Curve for Sheet 1.

Table 5
Parameter Optimization and Function Maximization for Sheet 2.

Algorithm	GWO	EO	MPA	KMA	SaDE	WSO	RIME	TEO	GA	BfOA
ξ_1	−1.19513	−0.85357	−0.86624	−0.87838	−0.88073	−1.12597	−1.04335	−1.0918	−0.89187	−0.85352
ξ_2	0.003501	0.002608	0.003305	0.002719	0.002934	0.003217	0.003202	0.00355	0.002775	0.002412
ξ_3	4.36E-05	5.09E-05	0.000098	5.37E-05	6.85E-05	3.77E-05	5.38E-05	6.86E-05	5.52E-05	3.69E-05
ξ_4	−9.5E-05	−9.5E-05	−9.5E-05	−9.5E-05	−9.5E-05	−9.5E-05	−9.5E-05	−9.5E-05	−9.5E-05	−9.5E-05
λ	14	14	14	14	14.09145	14	14	14.05581	14.15717	14
R_c	0.000131	0.000119	0.00012	0.000121	0.00013	0.000126	0.000116	0.000131	0.000112	0.00012
B	0.01499	0.017053	0.016788	0.016731	0.016492	0.01605	0.01762	0.015711	0.01714	0.016788
Min.	0.275581	0.275216	0.275211	0.275231	0.275921	0.275332	0.275454	0.276533	0.287704	0.275211
Max.	1.127451	0.333374	0.336021	0.307832	0.295055	0.317408	0.278103	0.287188	0.765945	0.275211
Mean	0.484872	0.298689	0.279138	0.284577	0.28261	0.2808	0.276357	0.280744	0.421136	0.275211
Std.	0.221139	0.017156	0.013776	0.012391	0.006287	0.009686	0.000687	0.003778	0.142411	3.78E-16
RT	16.79163	17.69071	15.48994	16.44445	32.77376	17.86023	19.24396	19.62964	34.30552	0.632919
FR	8.684211	7.105263	3.684211	4.578947	6	4.947368	3.894737	5.894737	9.210526	1

and MPA (0.036852). Its minimal standard deviation of SSE (1.8E-05) indicates its consistent ability to find optimal solutions, making it the most stable algorithm tested. BfOA also exhibited the fastest run time (0.480288), significantly outperforming EO (13.57184) and KMA (11.59972), highlighting its computational efficiency for real-time applications. Its top ranking in the Friedman's ranking (FR) (1.105263) confirms its overall superior performance across all metrics. Table 4 provides a comprehensive comparison between experimental and calculated data. The figures visually confirm BfOA's effectiveness. Fig. 2 (a) shows the close agreement between measured and estimated V—I and P—V characteristics. The error plot demonstrates consistently low absolute and relative errors across the entire current range, highlighting BfOA's robustness in modeling PEMFCs' non-linear behavior. Fig. 2(b)'s boxplot comparison of fitness values shows BfOA's tight clustering with no outliers and minimal spread, indicating superior stability and reliability compared to algorithms like GWO and GA, which exhibit greater

Table 6
Performance metrics of the Proposed algorithm for Sheet 2.

Vcell	Icell	Vest	AE	Pest	Pref	MBE	RE %
61.64	2.25	62.32708	0.687083	140.2359	138.69	0.016279	1.114671
59.57	6.75	59.75391	0.183906	403.3389	402.0975	0.001166	0.308722
58.94	9	59.02299	0.082995	531.207	530.46	0.000238	0.140813
57.54	15.75	57.47245	0.067553	905.191	906.255	0.000157	0.117401
56.8	20.25	56.69501	0.104994	1148.074	1150.2	0.00038	0.184848
56.13	24.75	56.02304	0.106962	1386.57	1389.218	0.000395	0.190562
55.23	31.5	55.13803	0.091967	1736.848	1739.745	0.000292	0.166516
54.66	36	54.60299	0.057007	1965.708	1967.76	0.000112	0.104294
53.61	45	53.61886	0.008863	2412.849	2412.45	2.71E-06	0.016533
52.86	51.75	52.93264	0.072643	2739.264	2735.505	0.000182	0.137426
51.91	67.5	51.43559	0.474414	3471.902	3503.925	0.007761	0.913916
51.22	72	51.02539	0.194606	3673.828	3687.84	0.001306	0.379942
49.66	90	49.42672	0.233283	4448.405	4469.4	0.001877	0.46976
49	99	48.64101	0.358993	4815.46	4851	0.004444	0.732639
48.15	105.8	48.04916	0.100837	5083.601	5094.27	0.000351	0.209422
47.52	110.3	47.6574	0.137396	5256.611	5241.456	0.000651	0.289134
47.1	117	47.07283	0.02717	5507.521	5510.7	2.55E-05	0.057687
46.48	126	46.28306	0.196943	5831.665	5856.48	0.001337	0.423715
45.66	135	45.4853	0.174696	6140.516	6164.1	0.001052	0.382603
44.85	141.8	44.87551	0.025509	6363.347	6359.73	2.24E-05	0.056876
44.24	150.8	44.05684	0.183157	6643.772	6671.392	0.001157	0.414008
42.45	162	43.01569	0.565692	6968.542	6876.9	0.011035	1.332607
41.66	171	42.15751	0.49751	7208.934	7123.86	0.008535	1.194214
40.68	182.3	41.04751	0.367506	7482.96	7415.964	0.004657	0.903408
40.09	189	40.36954	0.279538	7629.843	7577.01	0.002695	0.697275
39.51	195.8	39.66413	0.154127	7766.236	7736.058	0.000819	0.390097
38.73	204.8	38.69983	0.030168	7925.726	7931.904	3.14E-05	0.077892
38.15	211.5	37.95577	0.194228	8027.646	8068.725	0.001301	0.509117
37.38	220.5	36.91421	0.46579	8139.583	8242.29	0.007481	1.246095
			0.211225			**0.002612**	**0.453869**

variability. Finally, Fig. 2(c) shows BfOA's rapid convergence, stabilizing within the first 50 iterations, while MPA and KMA take longer. This smooth and efficient convergence demonstrates BfOA's ability to quickly and effectively minimize fitness values, a key advantage in optimization.

SHEET 2:

The BfOA excelled in optimizing the Sheet 2 PEMFC, providing accurate parameter estimates, fast convergence, and consistent results. Table 5 shows BfOA achieving the lowest mean (0.275211) and minimum (0.275211) SSE, surpassing both traditional algorithms like GA (0.421136) and GWO (0.484872), and newer ones like TEO (0.280744) and MPA (0.279138). Its minimal standard deviation of SSE (3.78E-16) indicates its consistent ability to find optimal solutions, making it the most stable algorithm tested. BfOA also exhibited the fastest run time (0.632919), significantly outperforming EO (17.69071) and KMA (16.44445), highlighting its computational efficiency for real-time applications. Its top ranking in the Friedman's ranking (FR) (1) confirms its overall superior performance across all metrics. Table 6 provides a comprehensive comparison between experimental and calculated data. The figures visually confirm BfOA's effectiveness. Fig. 3(a) shows the close agreement between measured and estimated V—I and P—V characteristics. The error plot demonstrates consistently low absolute and relative errors across the entire current range, highlighting BfOA's robustness in modeling PEMFCs' non-linear behavior. Fig. 3(b)'s boxplot comparison of fitness values shows BfOA's tight clustering with no outliers and minimal spread, indicating superior stability and reliability compared to algorithms like GWO and GA, which exhibit greater variability. Finally, Fig. 3(c) shows BfOA's rapid convergence, stabilizing within the first 50 iterations, while MPA and KMA take longer. This smooth and efficient convergence demonstrates BfOA's ability to quickly and effectively minimize fitness values, a key advantage in optimization.

The BfOA excelled in optimizing the Sheet 3 PEMFC, providing accurate parameter estimates, fast convergence, and consistent results. Table 7 shows BfOA achieving the lowest mean (0.242352) and minimum (0.242284) SSE, surpassing both traditional algorithms like GA (0.404388) and GWO (0.491547), and newer ones like TEO (0.24241) and MPA (0.244324). Its minimal standard deviation of SSE (0.000203) indicates its consistent ability to find optimal solutions, making it the most stable algorithm tested. BfOA also exhibited the fastest run time (0.499323), significantly outperforming EO (13.04109) and KMA (11.94825), highlighting its computational efficiency for real-time applications. Its top ranking in the Friedman's ranking (FR) (1.421053) confirms its overall superior performance across all metrics. Table 8 provides a comprehensive comparison between experimental and calculated data. The figures visually confirm BfOA's effectiveness. Fig. 4 (a) shows the close agreement between measured and estimated V—I and P—V characteristics. The error plot demonstrates consistently low absolute and relative errors across the entire current range, highlighting BfOA's robustness in modeling PEMFCs' non-linear behavior. Fig. 4(b)'s boxplot comparison of fitness values shows BfOA's tight clustering with no outliers and minimal spread, indicating superior stability and reliability compared to algorithms like GWO and GA, which exhibit greater variability. Finally, Fig. 4(c) shows BfOA's rapid convergence, stabilizing within the first 50 iterations, while MPA and KMA take longer. This smooth and efficient convergence demonstrates BfOA's ability to quickly and effectively minimize fitness values, a key advantage in optimization.

The BfOA excelled in optimizing the Sheet 4 PEMFC, providing accurate parameter estimates, fast convergence, and consistent results. Table 9 shows BfOA achieving the lowest mean (0.102915) and minimum (0.102915) SSE, surpassing both traditional algorithms like GA (0.10729) and GWO (0.104731), and newer ones like TEO (0.102918) and MPA (0.103268). Its minimal standard deviation of SSE (5.02E-16)

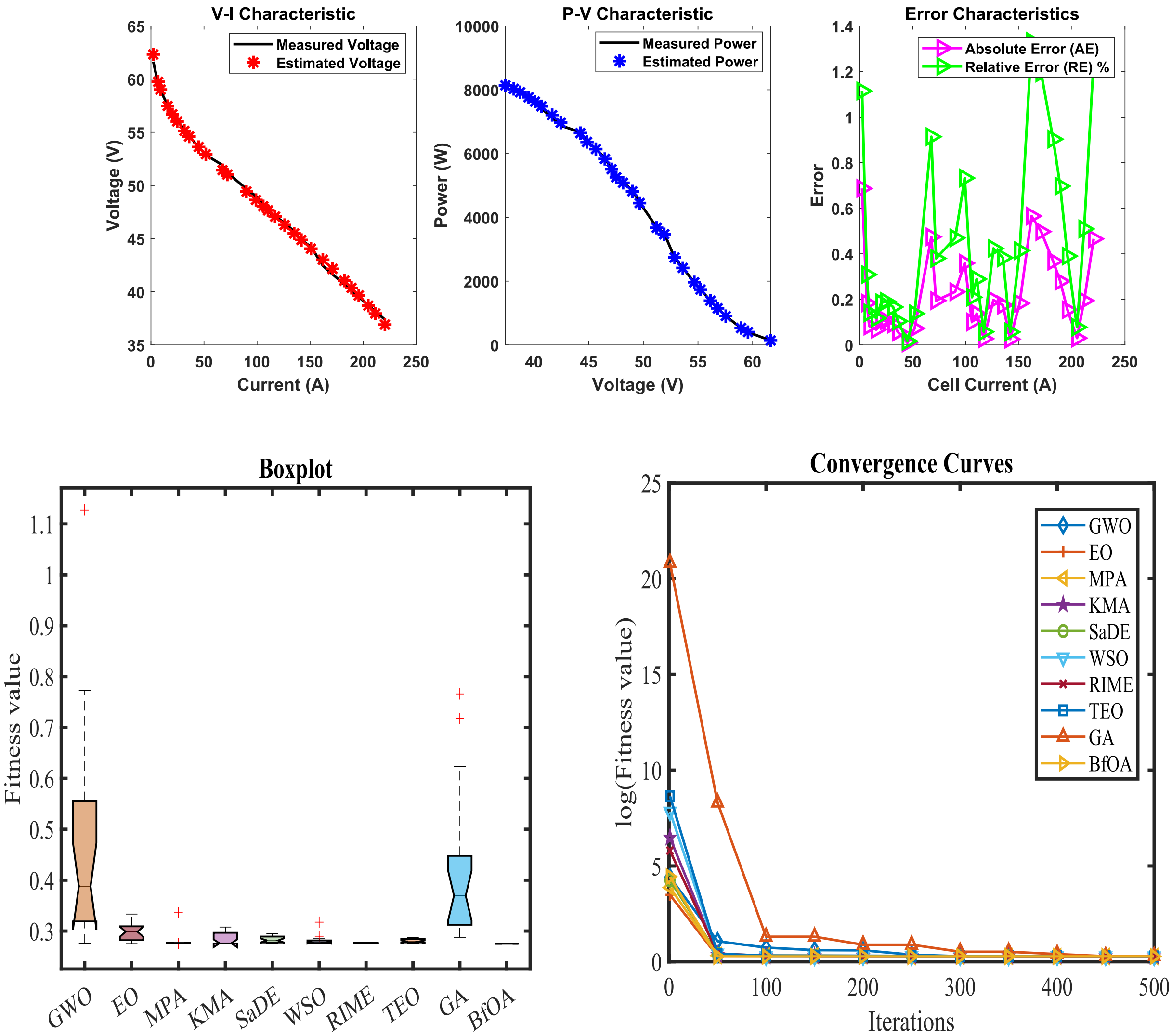

Fig. 3. Characteristic curves (a) P—V, V—I, and Error Curve, (b) Box-Plot (c) Convergence Curve for Sheet 2.
SHEET 3:

indicates its consistent ability to find optimal solutions, making it the most stable algorithm tested. BfOA also exhibited the fastest run time (0.418634), significantly outperforming EO (12.70402) and KMA (11.89375), highlighting its computational efficiency for real-time applications. Its top ranking in the Friedman's ranking (FR) (1.236842) confirms its overall superior performance across all metrics. Table 10 provides a comprehensive comparison between experimental and calculated data. The figures visually confirm BfOA's effectiveness. Fig. 5 (a) shows the close agreement between measured and estimated V—I and P—V characteristics. The error plot demonstrates consistently low absolute and relative errors across the entire current range, highlighting BfOA's robustness in modeling PEMFCs' non-linear behavior. Fig. 5(b)'s boxplot comparison of fitness values shows BfOA's tight clustering with no outliers and minimal spread, indicating superior stability and reliability compared to algorithms like GWO and GA, which exhibit greater variability. Finally, Fig. 5(c) shows BfOA's rapid convergence,

Table 7
Parameter Optimization and Function Maximization for Sheet 3.

Algorithm	GWO	EO	MPA	KMA	SaDE	WSO	RIME	TEO	GA	BfOA
ξ_1	−1.19915	−0.86356	−0.8532	−1.14048	−1.06004	−0.85471	−1.17106	−0.91178	−1.19457	−0.95911
ξ_2	0.004202	0.003251	0.002288	0.003627	0.003575	0.002301	0.003783	0.002804	0.004181	0.003268
ξ_3	9.03E-05	9.6E-05	0.000036	6.51E-05	7.77E-05	3.66E-05	6.89E-05	5.76E-05	8.98E-05	7.81E-05
ξ_4	−9.5E-05	−9.5E-05	−9.5E-05	−9.6E-05	−9.5E-05	−9.5E-05	−9.5E-05	−9.5E-05	−9.5E-05	−9.5E-05
λ	16.70864	22.99352	23	21.69911	22.77184	19.56966	22.84351	22.87037	22.19259	23
R_c	0.000795	0.000796	0.000673	0.000513	0.000641	0.000631	0.000673	0.000668	0.000608	0.000673
B	0.169976	0.172879	0.17532	0.177991	0.175863	0.174712	0.175362	0.17539	0.17714	0.17532
Min.	0.244111	0.242689	0.242284	0.24286	0.242316	0.24256	0.2423	0.24229	0.244627	0.242284
Max.	0.91361	0.246508	0.250432	0.24609	0.243161	0.248828	0.242626	0.242729	0.989933	0.242927
Mean	0.491547	0.243763	0.244324	0.244328	0.24263	0.244878	0.242451	0.24241	0.404388	0.242352
Std.	0.186746	0.000956	0.002102	0.00105	0.00022	0.001828	8.99E-05	0.000129	0.223497	0.000203
RT	12.6985	13.04109	11.45088	11.94825	24.19573	14.91282	13.1545	15.48517	25.33733	0.499323
FR	9.631579	5.894737	5.631579	6.736842	4	6.842105	2.947368	2.684211	9.210526	1.421053

Table 8
Performance metrics of the Proposed algorithm for Sheet 3.

Vcell	Icell	Vest	AE	Pest	Pref	MBE	RE %
43.17	1.004	43.34081	0.170809	43.51417	43.34268	0.001621	0.395667
41.14	3.166	41.09008	0.049922	130.0912	130.2492	0.000138	0.121347
40.09	5.019	39.91451	0.175488	200.3309	201.2117	0.001711	0.437735
39.04	7.027	38.85715	0.182848	273.0492	274.3341	0.001857	0.46836
37.99	8.958	37.93346	0.056535	339.808	340.3144	0.000178	0.148816
37.08	10.97	37.01454	0.065463	406.0495	406.7676	0.000238	0.176546
36.03	13.05	36.07991	0.049906	470.8428	470.1915	0.000138	0.138511
35.19	15.06	35.17136	0.018636	529.6807	529.9614	1.93E-05	0.052958
34.07	17.07	34.24209	0.172088	584.5124	581.5749	0.001645	0.505102
33.02	19.07	33.28313	0.263126	634.7092	629.6914	0.003846	0.796869
32.04	21.08	32.2707	0.2307	680.2664	675.4032	0.002957	0.720038
31.2	23.01	31.23769	0.037694	718.7793	717.912	7.89E-05	0.120813
29.8	24.94	30.12737	0.327372	751.3766	743.212	0.005954	1.098562
28.96	26.87	28.91713	0.042866	777.0034	778.1552	0.000102	0.148018
28.12	28.96	27.45776	0.662243	795.1766	814.3552	0.024365	2.355061
26.3	30.81	25.9918	0.308195	800.8075	810.303	0.005277	1.171846
24.06	32.97	23.98487	0.075131	790.7811	793.2582	0.000314	0.312265
21.4	34.9	21.78563	0.385634	760.3186	746.86	0.008262	1.802027
			0.181925			**0.003261**	**0.609475**

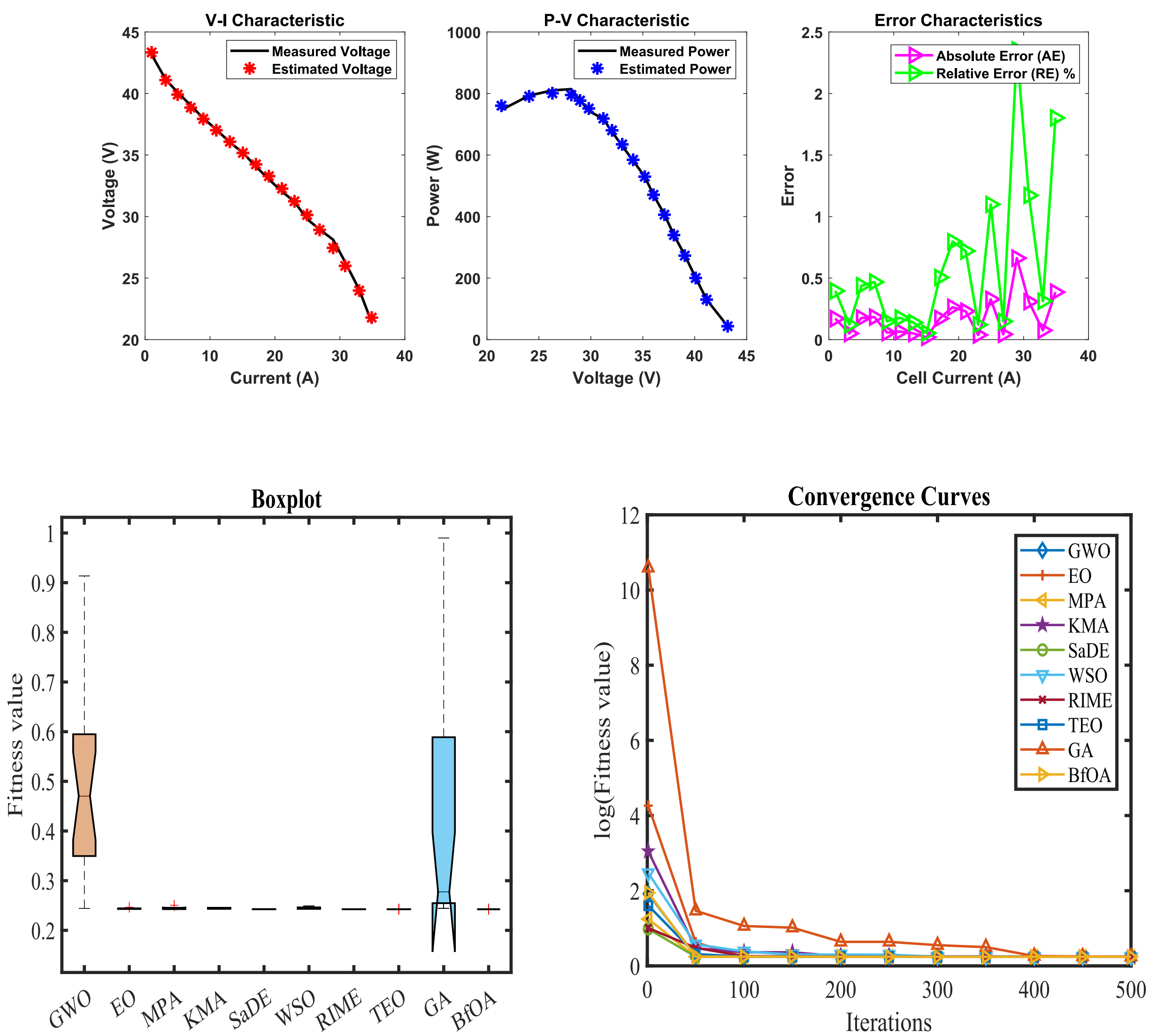

Fig. 4. Characteristic curves (a) P—V, V—I, and Error Curve, (b) Box-Plot (c) Convergence Curve for Sheet 3.

SHEET 4:

Table 9
Parameter Optimization and Function Maximization for Sheet 4.

Algorithm	GWO	EO	MPA	KMA	SaDE	WSO	RIME	TEO	GA	BfOA
ξ_1	−1.08243	−0.8532	−0.87323	−0.94108	−0.94759	−1.08444	−0.99978	−1.0995	−1.02245	−0.96125
ξ_2	0.002218	0.001509	0.001632	0.00204	0.002317	0.002802	0.001987	0.002508	0.002185	0.002705
ξ_3	0.000036	3.6E-05	4.04E-05	5.46E-05	7.31E-05	7.75E-05	3.78E-05	5.3E-05	4.7E-05	9.79E-05
ξ_4	−0.00011	−0.00011	−0.00011	−0.00011	−0.00011	−0.00011	−0.00011	−0.00011	−0.00011	−0.00011
λ	14	14	14	14.03889	14.00003	14.02883	14	14.0004	14.24745	14
R_c	0.0008	0.0008	0.0008	0.000788	0.0008	0.000498	0.0008	0.0008	0.000376	0.0008
B	0.0136	0.0136	0.0136	0.013647	0.0136	0.013738	0.0136	0.013601	0.0136	0.0136
Min.	0.102915	0.102915	0.102915	0.10295	0.102915	0.103258	0.102915	0.102916	0.103598	0.102915
Max.	0.111013	0.103523	0.105211	0.104156	0.103178	0.10501	0.102921	0.102924	0.116042	0.102915
Mean	0.104731	0.103061	0.103268	0.103437	0.102971	0.103928	0.102916	0.102918	0.10729	0.102915
Std.	0.002186	0.000225	0.000637	0.000299	6.26E-05	0.000471	1.85E-06	2.45E-06	0.003056	5.02E-16
RT	12.36721	12.70402	11.02456	11.89375	23.78162	13.1237	12.76383	14.96713	24.78275	0.418634
FR	7.263158	4.526316	3.552632	7.157895	5.421053	8.315789	3.368421	4.368421	9.789474	1.236842

Table 10
Performance metrics of the Proposed algorithm for Sheet 4.

Vcell	Icell	Vest	AE	Pest	Pref	MBE	RE %
9.58	0.104	9.755532	0.175532	1.014575	0.99632	0.001712	1.832272
9.42	0.2	9.435534	0.015534	1.887107	1.884	1.34E-05	0.164909
9.25	0.309	9.215306	0.034694	2.84753	2.85825	6.69E-05	0.37507
9.2	0.403	9.075995	0.124005	3.657626	3.7076	0.000854	1.347879
9.09	0.51	8.947893	0.142107	4.563425	4.6359	0.001122	1.563338
8.95	0.614	8.842715	0.107285	5.429427	5.4953	0.000639	1.19872
8.85	0.703	8.762861	0.087139	6.160291	6.22155	0.000422	0.984618
8.74	0.806	8.678685	0.061315	6.99502	7.04444	0.000209	0.70154
8.65	0.908	8.601587	0.048413	7.810241	7.8542	0.00013	0.559683
8.45	1.076	8.483394	0.033394	9.128131	9.0922	6.2E-05	0.39519
8.41	1.127	8.448867	0.038867	9.521873	9.47807	8.39E-05	0.462156
8.2	1.288	8.341384	0.141384	10.7437	10.5616	0.001111	1.724194
8.12	1.39	8.272663	0.152663	11.499	11.2868	0.001295	1.880081
8.11	1.45	8.231198	0.121198	11.93524	11.7595	0.000816	1.494432
8.05	1.578	8.137515	0.087515	12.841	12.7029	0.000425	1.087138
7.99	1.707	8.028856	0.038856	13.70526	13.63893	8.39E-05	0.486306
7.95	1.815	7.912602	0.037398	14.36137	14.42925	7.77E-05	0.47041
7.94	1.9	7.777413	0.162587	14.77708	15.086	0.001469	2.047696
			0.089438			**0.000588**	**1.043091**

stabilizing within the first 50 iterations, while MPA and KMA take longer. This smooth and efficient convergence demonstrates BfOA's ability to quickly and effectively minimize fitness values, a key advantage in optimization.

SHEET 5:

The BfOA excelled in optimizing the Sheet 5 PEMFC, providing accurate parameter estimates, fast convergence, and consistent results. Table 11 shows BfOA achieving the lowest mean (0.148632) and minimum (0.148632) SSE, surpassing both traditional algorithms like GA (0.176739) and GWO (0.164046), and newer ones like TEO (0.148667) and MPA (0.151141). Its minimal standard deviation of SSE (6.28E-14) indicates its consistent ability to find optimal solutions, making it the most stable algorithm tested. BfOA also exhibited the fastest run time (0.395629), significantly outperforming EO (11.08167) and KMA (10.86), highlighting its computational efficiency for real-time applications. Its top ranking in the Friedman's ranking (FR) (1.052632) confirms its overall superior performance across all metrics. Table 12 provides a comprehensive comparison between experimental and calculated data. The figures visually confirm BfOA's effectiveness. Fig. 6 (a) shows the close agreement between measured and estimated V—I and P—V characteristics. The error plot demonstrates consistently low absolute and relative errors across the entire current range, highlighting BfOA's robustness in modeling PEMFCs' non-linear behavior. Fig. 6(b)'s boxplot comparison of fitness values shows BfOA's tight clustering with no outliers and minimal spread, indicating superior stability and reliability compared to algorithms like GWO and GA, which exhibit greater variability. Finally, Fig. 6(c) shows BfOA's rapid convergence, stabilizing within the first 50 iterations, while MPA and KMA take longer. This smooth and efficient convergence demonstrates BfOA's ability to quickly and effectively minimize fitness values, a key advantage in optimization.

SHEET 6:

The BfOA excelled in optimizing the Sheet 6 PEMFC, providing accurate parameter estimates, fast convergence, and consistent results. Table 13 shows BfOA achieving the lowest mean (0.283774) and minimum (0.283774) SSE, surpassing both traditional algorithms like GA (0.343298) and GWO (0.33012), and newer ones like TEO (0.283813) and MPA (0.289831). Its minimal standard deviation of SSE (7.45E-16) indicates its consistent ability to find optimal solutions, making it the most stable algorithm tested. BfOA also exhibited the fastest run time (1.131579), significantly outperforming EO (16.46548) and KMA (8.558865), highlighting its computational efficiency for real-time applications. Its top ranking in the Friedman's ranking (FR) (1.131579) confirms its overall superior performance across all metrics. Table 14 provides a comprehensive comparison between experimental and calculated data. The figures visually confirm BfOA's effectiveness. Fig. 7 (a) shows the close agreement between measured and estimated V—I and P—V characteristics. The error plot demonstrates consistently low

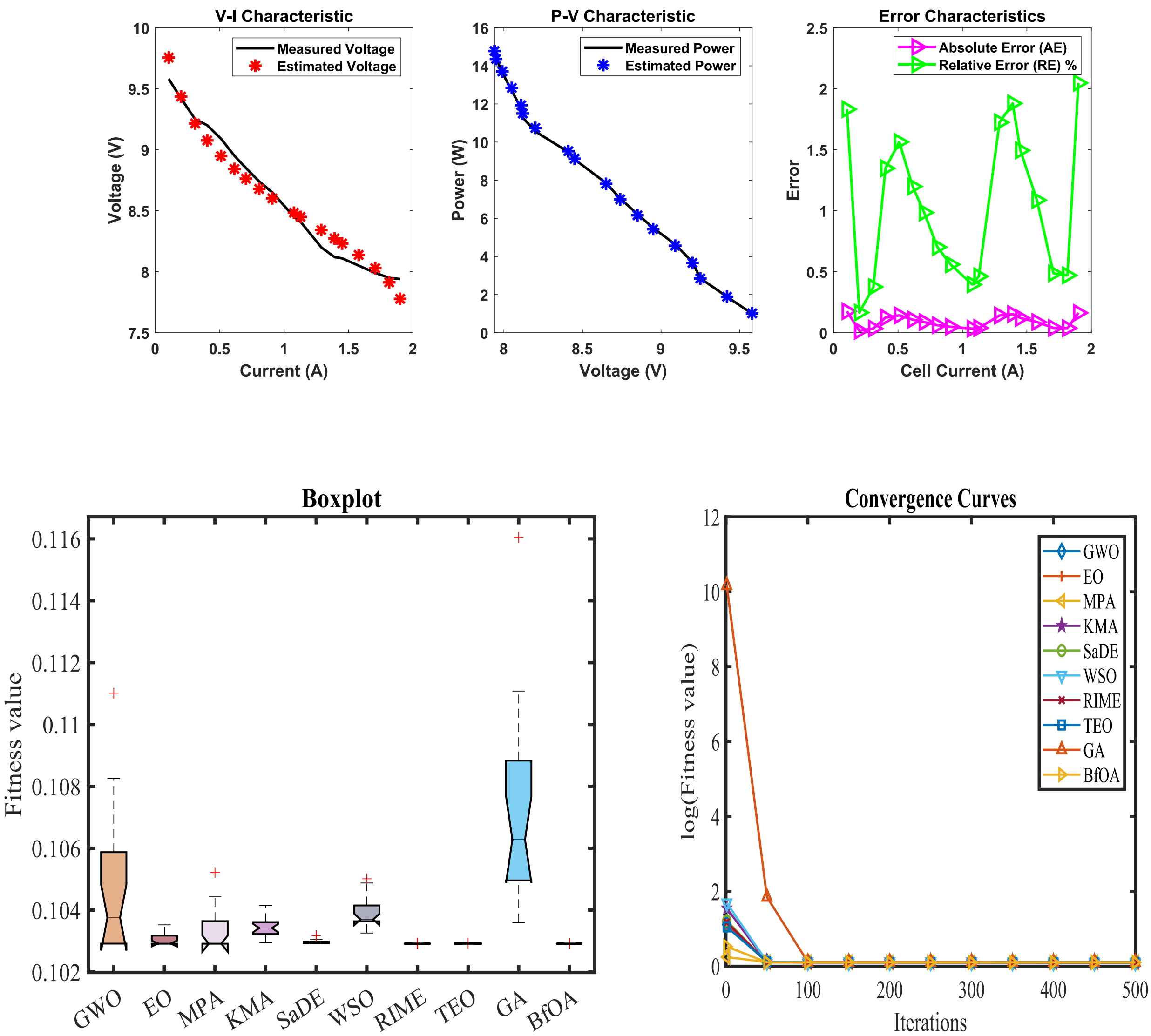

Fig. 5. Characteristic curves (a) P—V, V—I, and Error Curve, (b) Box-Plot (c) Convergence Curve for Sheet 4.

Table 11
Parameter Optimization and Function Maximization for Sheet 5.

Algorithm	GWO	EO	MPA	KMA	SaDE	WSO	RIME	TEO	GA	BfOA
ξ_1	−1.19969	−1.05297	−1.19969	−0.96195	−1.09597	−1.03132	−1.18075	−1.04667	−1.11406	−1.176
ξ_2	0.003948	0.003069	0.004082	0.002607	0.003751	0.003054	0.004072	0.003291	0.00377	0.004057
ξ_3	8.46E-05	5.23E-05	9.4E-05	3.82E-05	9.2E-05	5.56E-05	9.73E-05	6.94E-05	8.94E-05	9.72E-05
ξ_4	−0.00017	−0.00017	−0.00017	−0.00017	−0.00017	−0.00017	−0.00017	−0.00017	−0.00017	−0.00017
λ	14.28159	14.55083	14.43913	14.43219	14.45916	14.68177	14.46568	14.42504	14.75997	14.43913
R_c	0.000149	0.000215	0.0001	0.000107	0.0001	0.000125	0.0001	0.000101	0.000325	0.0001
B	0.01405	0.013606	0.013795	0.013819	0.013839	0.01409	0.013892	0.013775	0.0136	0.013795
Min.	0.149602	0.148839	0.148632	0.148661	0.148633	0.148723	0.148648	0.148633	0.149372	0.148632
Max.	0.186279	0.15686	0.161938	0.151153	0.149569	0.167279	0.149008	0.148926	0.292068	0.148632
Mean	0.164046	0.151521	0.151141	0.149497	0.148975	0.151333	0.14874	0.148667	0.176739	0.148632
Std.	0.010976	0.002961	0.004822	0.000686	0.00029	0.004437	8.82E-05	6.89E-05	0.032686	6.28E-14
RT	11.0179	11.08167	9.775574	10.86	21.22951	11.92743	11.51818	14.01454	22.13422	0.395629
FR	9.157895	7.105263	5.263158	5.789474	4.526316	6.526316	3.789474	2.578947	9.210526	1.052632

Table 12
Performance metrics of the Proposed algorithm for Sheet 5.

Vcell	Icell	Vest	AE	Pest	Pref	MBE	RE %
23.5	0.5	23.48309	0.016914	11.74154	11.75	1.91E-05	0.071975
21.5	2.1	21.2513	0.248696	44.62774	45.15	0.004123	1.156727
20.5	2.8	20.75981	0.259815	58.12748	57.4	0.0045	1.267389
19.9	4	20.10958	0.209577	80.43831	79.6	0.002928	1.053152
19.5	5.7	19.39753	0.102468	110.5659	111.15	0.0007	0.525477
19	7.1	18.90725	0.092746	134.2415	134.9	0.000573	0.488139
18.5	8	18.61964	0.11964	148.9571	148	0.000954	0.646705
17.8	11.1	17.72275	0.077246	196.7226	197.58	0.000398	0.433969
17.3	13.7	17.02409	0.275911	233.23	237.01	0.005075	1.594863
16.2	16.5	16.27464	0.074644	268.5316	267.3	0.000371	0.460763
15.9	17.5	15.99828	0.09828	279.9699	278.25	0.000644	0.618116
15.5	18.9	15.59366	0.093658	294.7201	292.95	0.000585	0.604245
15.1	20.3	15.15114	0.05114	307.5681	306.53	0.000174	0.338674
14.6	22	14.47819	0.121813	318.5201	321.2	0.000989	0.834336
13.8	22.9	13.82904	0.029041	316.685	316.02	5.62E-05	0.210444
			0.124773			**0.001473**	**0.686998**

absolute and relative errors across the entire current range, highlighting BfOA's robustness in modeling PEMFCs' non-linear behavior. Fig. 7(b)'s boxplot comparison of fitness values shows BfOA's tight clustering with no outliers and minimal spread, indicating superior stability and reliability compared to algorithms like GWO and GA, which exhibit greater variability. Finally, Fig. 7(c) shows BfOA's rapid convergence, stabilizing within the first 50 iterations, while MPA and KMA take longer. This smooth and efficient convergence demonstrates BfOA's ability to quickly and effectively minimize fitness values, a key advantage in optimization.

SHEET 7:

The BfOA excelled in optimizing the Sheet 7 PEMFC, providing accurate parameter estimates, fast convergence, and consistent results. Table 15 shows BfOA achieving the lowest mean (0.121755) and minimum (0.121755) SSE, surpassing both traditional algorithms like GA (0.246158) and GWO (0.143066), and newer ones like TEO (0.12177) and MPA (0.130624). Its minimal standard deviation of SSE (7.83E-14) indicates its consistent ability to find optimal solutions, making it the most stable algorithm tested. BfOA also exhibited the fastest run time (0.415718), significantly outperforming EO (11.21283) and KMA (9.10505), highlighting its computational efficiency for real-time applications. Its top ranking in the Friedman's ranking (FR) (1.078947) confirms its overall superior performance across all metrics. Table 16 provides a comprehensive comparison between experimental and calculated data. The figures visually confirm BfOA's effectiveness. Fig. 8 (a) shows the close agreement between measured and estimated V—I and P—V characteristics. The error plot demonstrates consistently low absolute and relative errors across the entire current range, highlighting BfOA's robustness in modeling PEMFCs' non-linear behavior. Fig. 8(b)'s boxplot comparison of fitness values shows BfOA's tight clustering with no outliers and minimal spread, indicating superior stability and reliability compared to algorithms like GWO and GA, which exhibit greater variability. Finally, Fig. 8(c) shows BfOA's rapid convergence, stabilizing within the first 50 iterations, while MPA and KMA take longer. This smooth and efficient convergence demonstrates BfOA's ability to quickly and effectively minimize fitness values, a key advantage in optimization.

SHEET 8:

The BfOA excelled in optimizing the Sheet 8 PEMFC, providing accurate parameter estimates, fast convergence, and consistent results. Table 17 shows BfOA achieving the lowest mean (0.078492) and minimum (0.078492) SSE, surpassing both traditional algorithms like GA (0.154449) and GWO (0.100292), and newer ones like TEO (0.078519) and MPA (0.092949). Its minimal standard deviation of SSE (1.07E-15) indicates its consistent ability to find optimal solutions, making it the most stable algorithm tested. BfOA also exhibited the fastest run time (0.400847), significantly outperforming EO (11.13641) and KMA (8.698193), highlighting its computational efficiency for real-time applications. Its top ranking in the Friedman's ranking (FR) (1) confirms its overall superior performance across all metrics. Table 18 provides a comprehensive comparison between experimental and calculated data. The figures visually confirm BfOA's effectiveness. Fig. 9(a) shows the close agreement between measured and estimated V—I and P—V characteristics. The error plot demonstrates consistently low absolute and

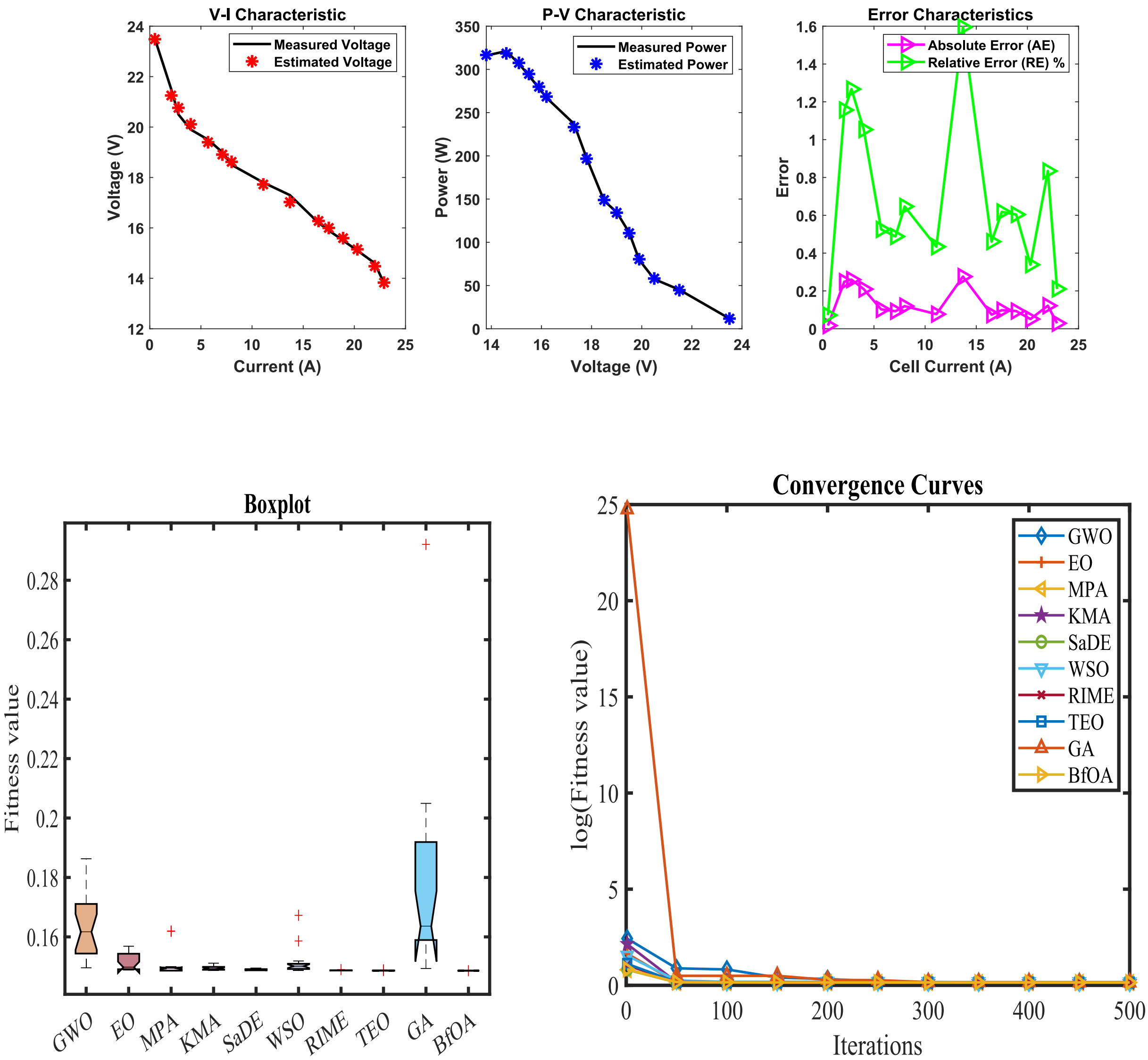

Fig. 6. Characteristic curves (a) P—V, V—I, and Error Curve, (b) Box-Plot (c) Convergence Curve for Sheet 5.

Table 13
Parameter Optimization and Function Maximization for Sheet 6.

Algorithm	GWO	EO	MPA	KMA	SaDE	WSO	RIME	TEO	GA	BfOA
ξ_1	−0.8532	−1.19969	−1.19969	−0.85905	−0.98106	−0.92629	−1.015	−1.09248	−1.19969	−1.12213
ξ_2	0.002182	0.002902	0.00377	0.002121	0.002348	0.002144	0.002627	0.002937	0.003742	0.002673
ξ_3	5.73E-05	3.6E-05	0.000098	5.22E-05	4.27E-05	3.96E-05	5.54E-05	6.12E-05	9.55E-05	3.6E-05
ξ_4	−0.00018	−0.00017	−0.00017	−0.00017	−0.00017	−0.00017	−0.00017	−0.00017	−0.00018	−0.00017
λ	14	14	14	14	14	14	14	14.00003	18.98273	14
R_c	0.0008	0.0008	0.0008	0.0008	0.0008	0.0008	0.0008	0.0008	0.000673	0.0008
B	0.015466	0.017318	0.017317	0.017244	0.017317	0.017282	0.017308	0.017344	0.017796	0.017317
Min.	0.292313	0.283774	0.283774	0.283798	0.283774	0.283887	0.283774	0.28378	0.305328	0.283774
Max.	0.388926	0.319359	0.343183	0.337824	0.284766	0.340552	0.283991	0.283901	0.448243	0.283774
Mean	0.33012	0.288781	0.289831	0.30295	0.283917	0.310738	0.283824	0.283813	0.343298	0.283774
Std.	0.033056	0.010912	0.014156	0.019269	0.000286	0.020819	6.39E-05	3.3E-05	0.037873	7.45E-16
RT	953.4759	16.46548	7.315551	8.558865	16.23185	9.031189	9.27304	18.33893	22.29405	0.550266
FR	8.578947	4.263158	3.342105	7.052632	4.157895	7.947368	4.526316	4.684211	9.315789	1.131579

Table 14
Performance metrics of the Proposed algorithm for Sheet 6.

Vcell	Icell	Vest	AE	Pest	Pref	MBE	RE %
29.37	0.6	29.7147	0.344698	17.82882	17.622	0.00914	1.17364
26.77739	2.5	26.62879	0.148596	66.57198	66.94348	0.001699	0.554931
25.29025	5	25.00559	0.284663	125.0279	126.4513	0.006233	1.125585
24.28186	7.5	23.96352	0.318339	179.7264	182.1139	0.007795	1.311014
23.418	10	23.14754	0.270455	231.4754	234.18	0.005627	1.154903
22.7391	12	22.57673	0.162374	270.9208	272.8692	0.002028	0.714072
22.05852	14	22.04306	0.015467	308.6028	308.8193	1.84E-05	0.070117
21.38615	16	21.52088	0.134734	344.3341	342.1784	0.001396	0.630007
20.72173	18	20.98016	0.258429	377.6428	372.9911	0.005137	1.247139
20.026	20	20.364	0.337999	407.28	400.52	0.008788	1.687803
19.63635	21	19.98091	0.344565	419.5992	412.3634	0.009133	1.75473
19.19181	22	19.45678	0.264976	428.0492	422.2198	0.005401	1.380673
18.66363	23	18.17812	0.485508	418.0968	429.2635	0.018132	2.60136
			0.259293			**0.006194**	**1.185075**

relative errors across the entire current range, highlighting BfOA's robustness in modeling PEMFCs' non-linear behavior. Fig. 9(b)'s boxplot comparison of fitness values shows BfOA's tight clustering with no outliers and minimal spread, indicating superior stability and reliability compared to algorithms like GWO and GA, which exhibit greater variability. Finally, Fig. 9(c) shows BfOA's rapid convergence, stabilizing within the first 50 iterations, while MPA and KMA take longer. This smooth and efficient convergence demonstrates BfOA's ability to quickly and effectively minimize fitness values, a key advantage in optimization.

SHEET 9:

The BfOA excelled in optimizing the Sheet 9 PEMFC, providing accurate parameter estimates, fast convergence, and consistent results. Table 19 shows BfOA achieving the lowest mean (0.202319) and minimum (0.202319) SSE, surpassing both traditional algorithms like GA (0.31485) and GWO (0.214363), and newer ones like TEO (0.202332) and MPA (0.207943). Its minimal standard deviation of SSE (4.93E-16) indicates its consistent ability to find optimal solutions, making it the most stable algorithm tested. BfOA also exhibited the fastest run time (0.409435), significantly outperforming EO (8.864086) and KMA (8.350974), highlighting its computational efficiency for real-time applications. Its top ranking in the Friedman's ranking (FR) (1.157895) confirms its overall superior performance across all metrics. Table 20 provides a comprehensive comparison between experimental and calculated data. The figures visually confirm BfOA's effectiveness. Fig. 10(a) shows the close agreement between measured and estimated V—I and P—V characteristics. The error plot demonstrates consistently low absolute and relative errors across the entire current range, highlighting BfOA's robustness in modeling PEMFCs' non-linear behavior. Fig. 10(b)'s boxplot comparison of fitness values shows BfOA's tight clustering with no outliers and minimal spread, indicating superior stability and reliability compared to algorithms like GWO and GA, which exhibit greater variability. Finally, Fig. 10(c) shows BfOA's rapid convergence, stabilizing within the first 50 iterations, while MPA and KMA take longer. This smooth and efficient convergence demonstrates BfOA's ability to quickly and effectively minimize fitness values, a key advantage in optimization.

SHEET 10:

The BfOA excelled in optimizing the Sheet 10 PEMFC, providing accurate parameter estimates, fast convergence, and consistent results. Table 21 shows BfOA achieving the lowest mean (0.104446) and minimum (0.104446) SSE, surpassing both traditional algorithms like GA (0.160156) and GWO (0.118975), and newer ones like TEO (0.104509) and MPA (0.112964). Its minimal standard deviation of SSE (3.29E-15) indicates its consistent ability to find optimal solutions, making it the most stable algorithm tested. BfOA also exhibited the fastest run time (0.383702), significantly outperforming EO (8.828214) and KMA (8.350757), highlighting its computational efficiency for real-time applications. Its top ranking in the Friedman's ranking (FR) (1.052632) confirms its overall superior performance across all metrics. Table 22 provides a comprehensive comparison between experimental and calculated data. The figures visually confirm BfOA's effectiveness. Fig. 11(a) shows the close agreement between measured and estimated V—I and P—V characteristics. The error plot demonstrates consistently low absolute and relative errors across the entire current range, highlighting BfOA's robustness in modeling PEMFCs' non-linear behavior. Fig. 11(b)'s boxplot comparison of fitness values shows BfOA's tight clustering with no outliers and minimal spread, indicating superior

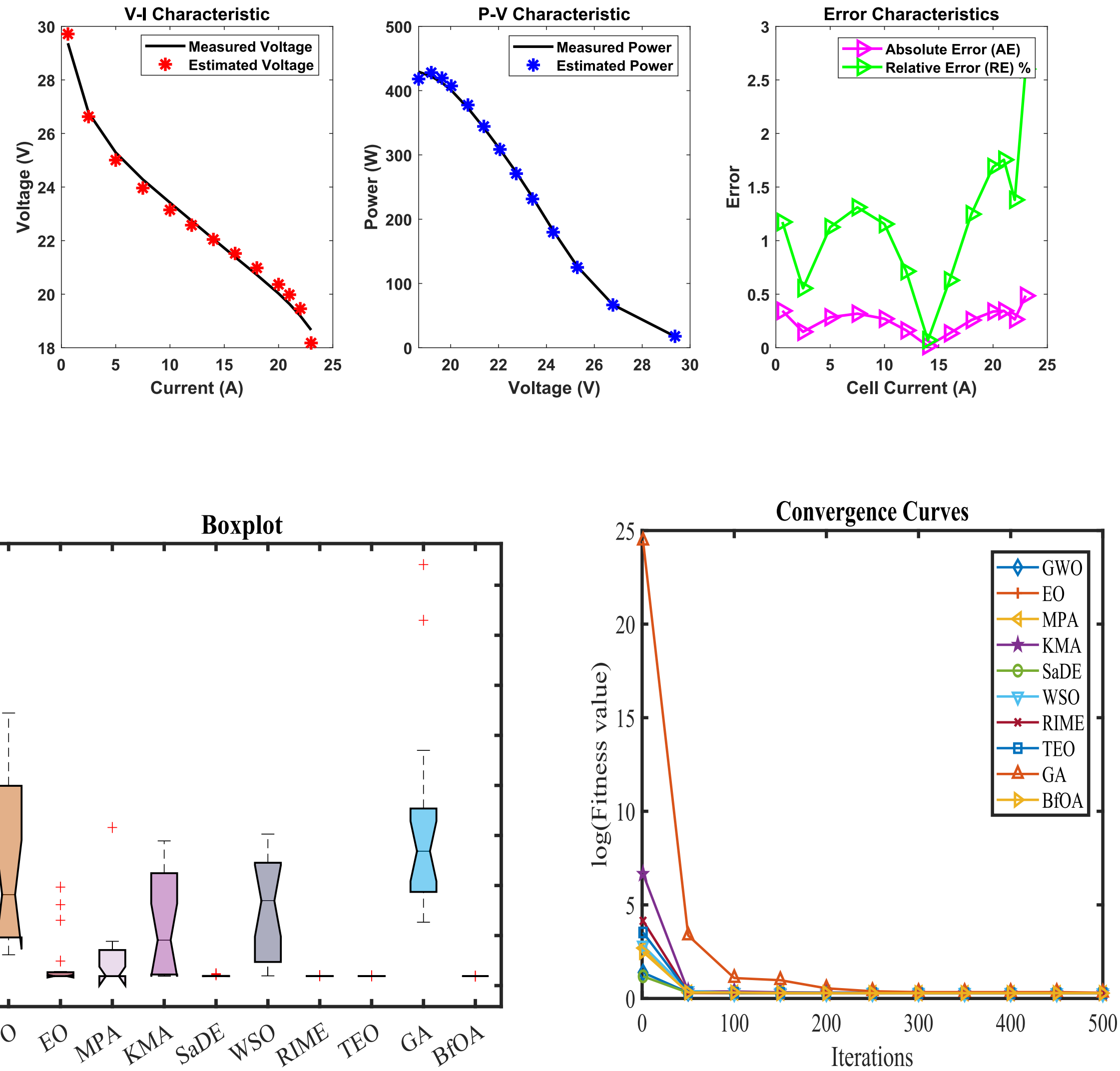

Fig. 7. Characteristic curves (a) P—V, V—I, and Error Curve, (b) Box-Plot (c) Convergence Curve for Sheet 6.

Table 15
Parameter Optimization and Function Maximization for Sheet 7.

Algorithm	GWO	EO	MPA	KMA	SaDE	WSO	RIME	TEO	GA	BfOA
ξ_1	−0.85857	−1.10021	−0.93543	−1.15625	−1.0749	−1.14392	−1.17057	−1.06456	−1.17805	−0.90506
ξ_2	0.002873	0.002788	0.003095	0.003316	0.003134	0.003198	0.003468	0.002896	0.003672	0.002163
ξ_3	0.000098	4.02E-05	0.000098	6.68E-05	7.1E-05	6.08E-05	7.5E-05	5.57E-05	8.78E-05	0.000036
ξ_4	−0.00015	−0.00015	−0.00015	−0.00015	−0.00015	−0.00015	−0.00015	−0.00015	−0.00015	−0.00015
λ	21.41057	23	23	23	23	22.69325	23	22.99859	20.19055	23
R_c	0.0001	0.00011	0.0001	0.000102	0.0001	0.000106	0.0001	0.0001	0.000372	0.0001
B	0.049994	0.050942	0.050979	0.050873	0.05098	0.051107	0.051032	0.050973	0.047043	0.050979
Min.	0.124617	0.121876	0.121755	0.121903	0.121755	0.122503	0.121769	0.121758	0.138036	0.121755
Max.	0.177992	0.130447	0.134718	0.131402	0.122945	0.156995	0.12328	0.121798	0.458087	0.121755
Mean	0.143066	0.126156	0.130624	0.124305	0.121975	0.129501	0.122114	0.12177	0.246158	0.121755
Std.	0.015666	0.002707	0.006191	0.002628	0.000408	0.008891	0.000356	1.07E-05	0.09787	7.83E-14
RT	13.94871	11.21283	11.07551	9.10505	17.89869	10.71752	11.62771	11.1221	16.82142	0.415718
FR	8.526316	6.473684	6.184211	5.684211	3.210526	6.894737	4.105263	2.947368	9.894737	1.078947

stability and reliability compared to algorithms like GWO and GA, which exhibit greater variability. Finally, Fig. 11(c) shows BfOA's rapid convergence, stabilizing within the first 50 iterations, while MPA and KMA take longer. This smooth and efficient convergence demonstrates BfOA's ability to quickly and effectively minimize fitness values, a key advantage in optimization.

SHEET 11:

The BfOA excelled in optimizing the Sheet 11 PEMFC, providing accurate parameter estimates, fast convergence, and consistent results. Table 23 shows BfOA achieving the lowest mean (0.075615) and minimum (0.075484) SSE, surpassing both traditional algorithms like GA (0.099695) and GWO (0.081158), and newer ones like TEO (0.075489)

Table 16
Performance metrics of the Proposed algorithm for Sheet 7.

Vcell	Icell	Vest	AE	Pest	Pref	MBE	RE %
22.6916	0.2417	22.56459	0.127013	5.453861	5.48456	0.001075	0.559736
20.1869	1.3177	20.35845	0.171555	26.82634	26.60028	0.001962	0.849833
19.2897	2.6819	19.32465	0.034945	51.82677	51.73305	8.14E-05	0.18116
18.5607	4.0118	18.66664	0.105942	74.88683	74.46182	0.000748	0.570787
18.1682	5.3755	18.13216	0.03604	97.46943	97.66316	8.66E-05	0.198369
17.7196	6.7563	17.66513	0.054469	119.3509	119.7189	0.000198	0.307396
17.271	8.0689	17.26039	0.010608	139.2724	139.358	7.5E-06	0.06142
16.4299	10.8134	16.47265	0.042753	178.1254	177.6631	0.000122	0.260212
15.7009	13.4556	15.72573	0.02483	211.5991	211.265	4.11E-05	0.158146
14.9907	16.1488	14.90759	0.083107	240.7397	242.0818	0.00046	0.554389
14.6542	17.5295	14.43437	0.219834	253.0272	256.8808	0.003222	1.500145
14.0374	18.8423	13.92017	0.117233	262.288	264.4969	0.000916	0.835145
13.1963	20.2234	13.25588	0.059584	268.079	266.8741	0.000237	0.45152
12.0187	21.6049	12.30085	0.282153	265.7587	259.6628	0.005307	2.347615
10.1308	22.9189	10.05734	0.073458	230.5032	232.1868	0.00036	0.725094
			0.096235			**0.000988**	**0.637398**

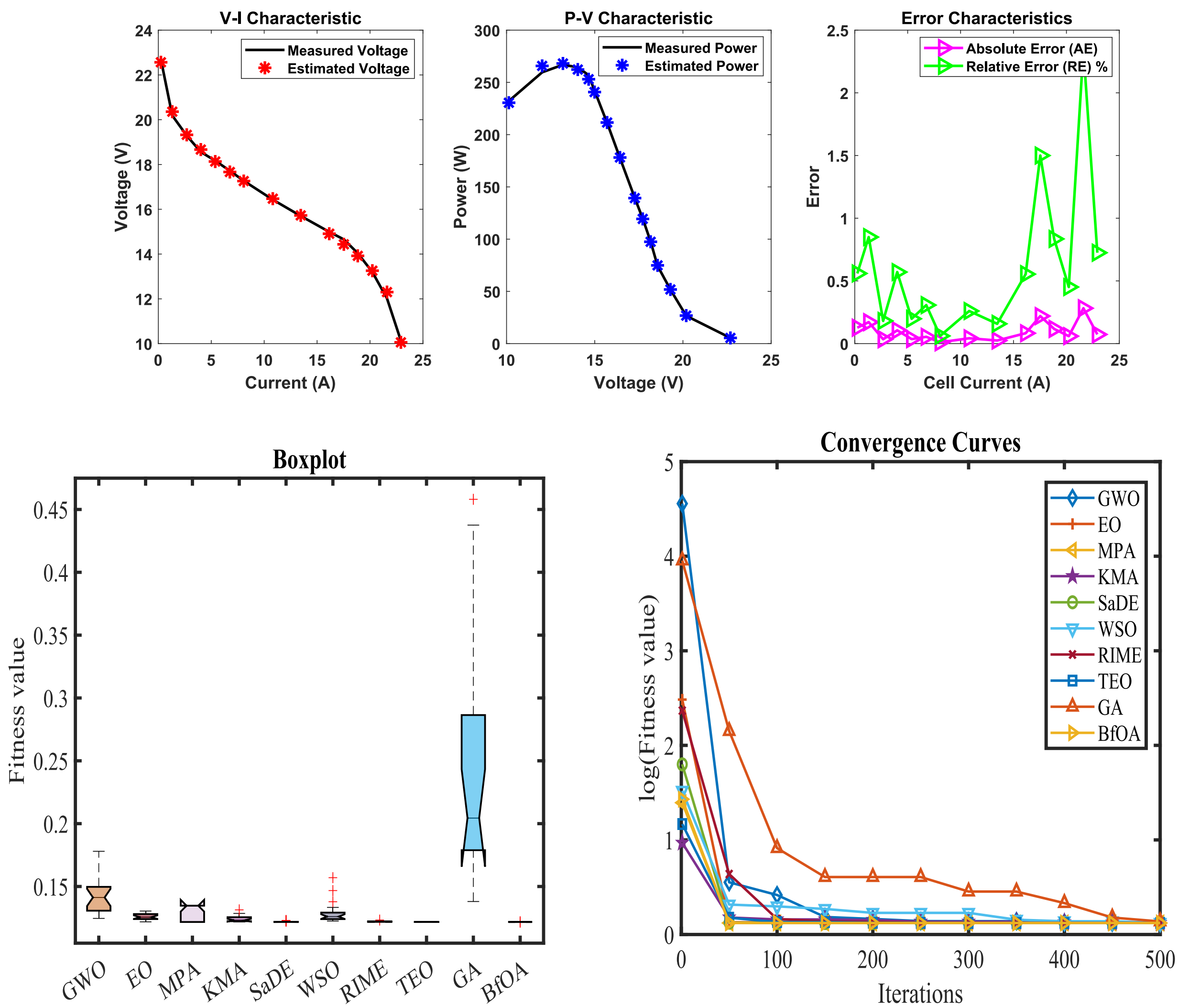

Fig. 8. Characteristic curves (a) P—V, V—I, and Error Curve, (b) Box-Plot (c) Convergence Curve for Sheet 7.

Table 17
Parameter Optimization and Function Maximization for Sheet 8.

Algorithm	GWO	EO	MPA	KMA	SaDE	WSO	RIME	TEO	GA	BfOA
ξ_1	−1.06562	−0.88706	−1.19969	−1.12047	−1.12024	−1.06201	−0.89457	−1.1477	−1.16338	−0.86113
ξ_2	0.003063	0.002537	0.003077	0.002978	0.003132	0.002892	0.002454	0.00313	0.003219	0.002099
ξ_3	6.67E-05	6.66E-05	3.79E-05	4.8E-05	6E-05	5.45E-05	5.85E-05	5.37E-05	5.73E-05	3.85E-05
ξ_4	−0.00015	−0.00015	−0.00015	−0.00015	−0.00015	−0.00015	−0.00015	−0.00015	−0.00014	−0.00015
λ	16.70538	14.16824	14.39771	14.37306	14.39421	14.44381	14.29039	14.42108	14.51394	14.39771
R_c	0.0008	0.000103	0.0001	0.000233	0.000104	0.000126	0.0001	0.0001	0.000346	0.0001
B	0.024465	0.023498	0.023974	0.023327	0.023961	0.023911	0.023847	0.02401	0.023133	0.023974
Min.	0.082987	0.078674	0.078492	0.079317	0.078508	0.078865	0.07855	0.078495	0.086535	0.078492
Max.	0.144733	0.092178	0.17633	0.082725	0.07991	0.108552	0.079064	0.078648	0.279766	0.078492
Mean	0.100292	0.082964	0.092949	0.080544	0.078983	0.08392	0.078811	0.078519	0.154449	0.078492
Std.	0.016436	0.003852	0.027937	0.000816	0.000498	0.00708	0.000159	3.81E-05	0.059497	1.07E-15
RT	8.771467	11.13641	8.146602	8.698193	16.63866	18.69854	8.989659	10.78804	17.06223	0.400847
FR	8.789474	6.894737	5.947368	6.157895	4	6.631579	3.842105	2.210526	9.526316	1

Table 18
Performance metrics of the Proposed algorithm for Sheet 8.

Vcell	Icell	Vest	AE	Pest	Pref	MBE	RE %
23.271	0.2582	23.21664	0.054362	5.994536	6.008572	0.000197	0.233603
21.028	1.334	21.10731	0.07931	28.15715	28.05135	0.000419	0.377162
20.0748	2.6471	20.11794	0.043141	53.2542	53.14	0.000124	0.214901
19.4019	4.0281	19.43404	0.032136	78.28224	78.15279	6.88E-05	0.165632
18.8972	5.3919	18.90022	0.003018	101.9081	101.8918	6.07E-07	0.015969
18.5047	6.7726	18.4333	0.071404	124.8413	125.3249	0.00034	0.385869
18.0561	8.0852	18.02927	0.026832	145.7702	145.9872	4.8E-05	0.148601
17.2897	10.8297	17.24932	0.040375	186.805	187.2423	0.000109	0.233523
16.5047	13.523	16.51247	0.007774	223.2982	223.1931	4.03E-06	0.047103
15.7196	16.1652	15.76837	0.048774	254.8989	254.1105	0.000159	0.310273
15.3271	17.5459	15.35272	0.025619	269.3773	268.9278	4.38E-05	0.167146
14.9907	18.8584	14.92473	0.06597	281.4565	282.7006	0.00029	0.440075
14.5421	20.2733	14.39848	0.143623	291.9046	294.8164	0.001375	0.987639
13.5888	21.5523	13.79568	0.206881	297.3287	292.8699	0.002853	1.522436
12.5234	22.9337	12.47931	0.044085	286.1969	287.2079	0.00013	0.352021
			0.059554			**0.000411**	**0.373464**

and MPA (0.075701). Its minimal standard deviation of SSE (0.000259) indicates its consistent ability to find optimal solutions, making it the most stable algorithm tested. BfOA also exhibited the fastest run time (0.343401), significantly outperforming EO (9.18711) and KMA (8.55728), highlighting its computational efficiency for real-time applications. Its top ranking in the Friedman's ranking (FR) (2.578947) confirms its overall superior performance across all metrics. Table 24 provides a comprehensive comparison between experimental and calculated data. The figures visually confirm BfOA's effectiveness. Fig. 12(a) shows the close agreement between measured and estimated V—I and P—V characteristics. The error plot demonstrates consistently low absolute and relative errors across the entire current range, highlighting BfOA's robustness in modeling PEMFCs' non-linear behavior. Fig. 12(b)'s boxplot comparison of fitness values shows BfOA's tight clustering with no outliers and minimal spread, indicating superior stability and reliability compared to algorithms like GWO and GA, which exhibit greater variability. Finally, Fig. 12(c) shows BfOA's rapid convergence, stabilizing within the first 50 iterations, while MPA and KMA take longer. This smooth and efficient convergence demonstrates BfOA's ability to quickly and effectively minimize fitness values, a key advantage in optimization.

The atypical shape of the V—I curve in Fig. 12 (Sheet 11) is attributed to the specific operating conditions and design parameters of the Horizon H-12 PEMFC stack under low-temperature (302K) and low hydrogen partial pressure (0.4 bar). These conditions exacerbate mass transport limitations at higher current densities, leading to a more pronounced voltage drop. The observed deviation from conventional PEMFC polarization curves aligns with prior experimental studies on low-pressure systems, where reduced reactant availability accelerates concentration losses [44,62]. The BfOA-optimized model accurately captures this behavior, as evidenced by the low SSE (0.0756) and RE (<1.88 % across all points), confirming its capability to replicate non-ideal operational scenarios.

SHEET 12:

The BfOA excelled in optimizing the Sheet 12 PEMFC, providing accurate parameter estimates, fast convergence, and consistent results. Table 25 shows BfOA achieving the lowest mean (0.064194) and minimum (0.064194) SSE, surpassing both traditional algorithms like GA (0.080342) and GWO (0.071575), and newer ones like TEO (0.064201) and MPA (0.070516). Its minimal standard deviation of SSE (1.31E-16) indicates its consistent ability to find optimal solutions, making it the most stable algorithm tested. BfOA also exhibited the fastest run time (0.358489), significantly outperforming EO (8.793425) and KMA (8.243002), highlighting its computational efficiency for real-time applications. Its top ranking in the Friedman's ranking (FR) (1) confirms its overall superior performance across all metrics. Table 26 provides a comprehensive comparison between experimental and calculated data. The figures visually confirm BfOA's effectiveness. Fig. 13(a) shows the close agreement between measured and estimated V—I and P—V characteristics. The error plot demonstrates consistently low absolute and relative errors across the entire current range, highlighting BfOA's robustness in modeling PEMFCs' non-linear behavior. Fig. 13(b)'s

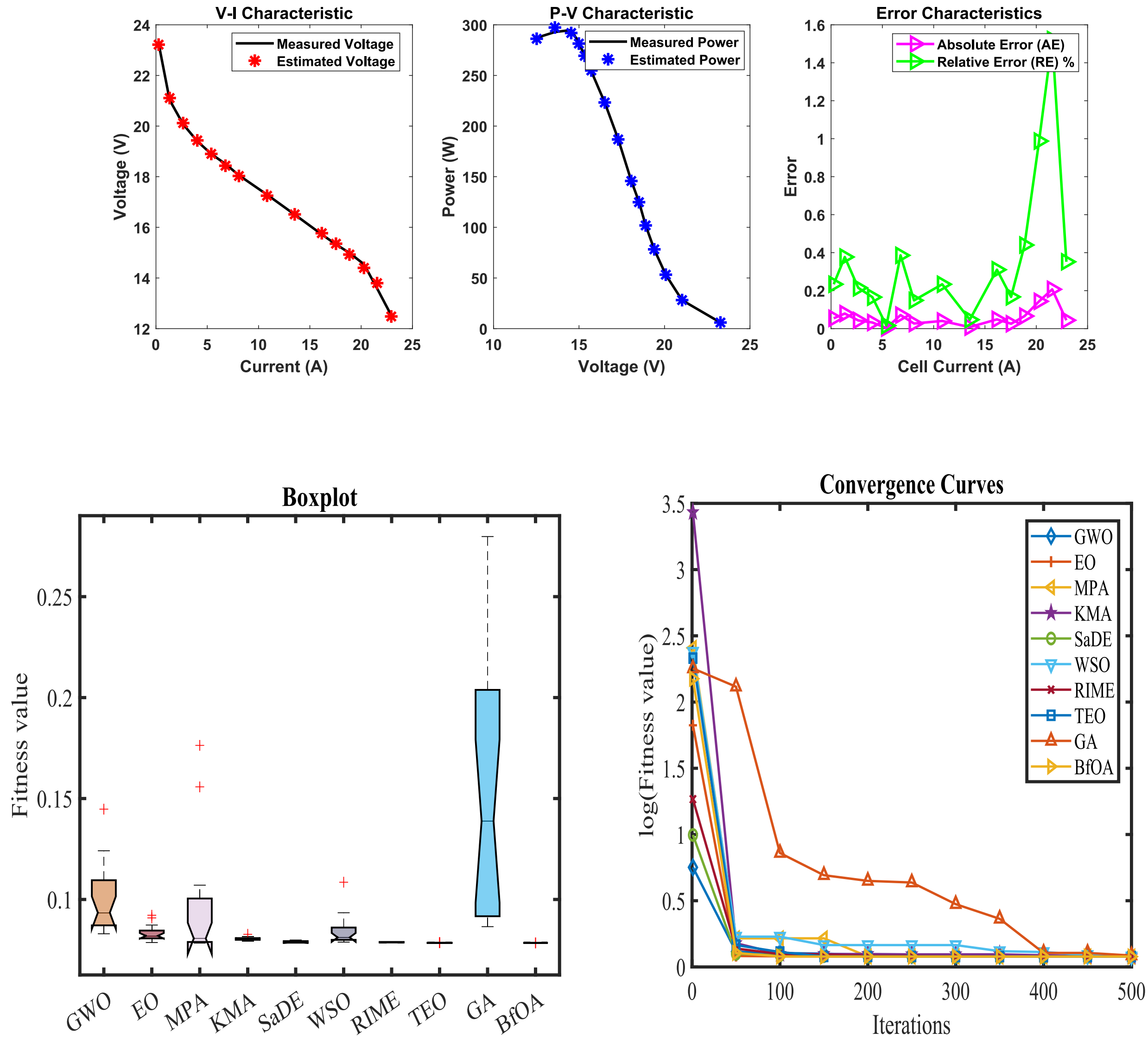

Fig. 9. Characteristic curves (a) P—V, V—I, and Error Curve, (b) Box-Plot (c) Convergence Curve for Sheet 8.

Table 19
Parameter Optimization and Function Maximization for Sheet 9.

Algorithm	GWO	EO	MPA	KMA	SaDE	WSO	RIME	TEO	GA	BfOA
ξ_1	−1.11541	−0.86148	−1.19969	−1.19045	−1.12918	−0.88025	−1.0156	−1.00268	−1.08762	−1.19969
ξ_2	0.00341	0.002066	0.003645	0.003605	0.002933	0.0027	0.002918	0.002593	0.002539	0.002861
ξ_3	0.000098	5.14E-05	9.73E-05	9.63E-05	5.81E-05	9.63E-05	8.26E-05	6.03E-05	0.000036	3.66E-05
ξ_4	−0.00012	−0.00012	−0.00012	−0.00012	−0.00012	−0.00012	−0.00012	−0.00012	−0.00011	−0.00012
λ	23	23	23	22.97141	22.99995	22.8007	23	22.99822	19.80597	23
R_c	0.000101	0.0001	0.0001	0.000124	0.0001	0.000101	0.0001	0.0001	0.000799	0.0001
B	0.061664	0.062477	0.06248	0.062212	0.062476	0.062191	0.062504	0.062495	0.057271	0.06248
Min.	0.20315	0.20232	0.202319	0.202522	0.202319	0.2026	0.202331	0.202322	0.221564	0.202319
Max.	0.232063	0.208651	0.242761	0.209289	0.203177	0.212069	0.203209	0.20235	0.66534	0.202319
Mean	0.214363	0.20432	0.207943	0.205125	0.202444	0.206712	0.202517	0.202332	0.31485	0.202319
Std.	0.008476	0.001837	0.009204	0.00205	0.000205	0.003035	0.000231	7.92E-06	0.111385	4.93E-16
RT	10.38317	8.864086	7.84418	8.350974	16.82277	9.316937	11.29366	10.77193	16.75946	0.409435
FR	8.157895	5.894737	5.157895	6.789474	3.842105	6.947368	4.210526	2.842105	10	1.157895

Table 20
Performance metrics of the Proposed algorithm for Sheet 9.

Vcell	Icell	Vest	AE	Pest	Pref	MBE	RE %
21.5139	0.2046	21.51968	0.005778	4.402926	4.401744	2.23E-06	0.026858
19.6737	1.2619	19.5779	0.095799	24.70535	24.82624	0.000612	0.486939
18.7154	2.6433	18.6624	0.053002	49.33032	49.47042	0.000187	0.283201
17.9449	3.9734	18.07571	0.130811	71.82203	71.30227	0.001141	0.728958
17.5497	5.3206	17.59286	0.043156	93.60455	93.37493	0.000124	0.245907
17.1545	6.7019	17.15542	0.000919	114.9739	114.9677	5.63E-08	0.005359
16.6843	8.0491	16.75861	0.07431	134.8917	134.2936	0.000368	0.445386
15.8752	10.7265	16.0031	0.127902	171.6573	170.2853	0.001091	0.805673
15.1411	13.472	15.212	0.070901	204.9361	203.9809	0.000335	0.46827
14.4634	16.1494	14.35228	0.111122	231.7807	233.5752	0.000823	0.768295
14.087	17.4795	13.85842	0.228581	242.2382	246.2337	0.003483	1.622638
13.5792	18.8438	13.26817	0.311027	250.0228	255.8837	0.006449	2.290463
12.6772	20.1739	12.54771	0.129485	253.1363	255.7486	0.001118	1.021403
10.8743	21.5382	11.47597	0.60167	247.1717	234.2128	0.024134	5.532958
8.9213	22.9025	8.794868	0.126432	201.4245	204.3201	0.001066	1.417191
			0.140726			**0.002729**	**1.076633**

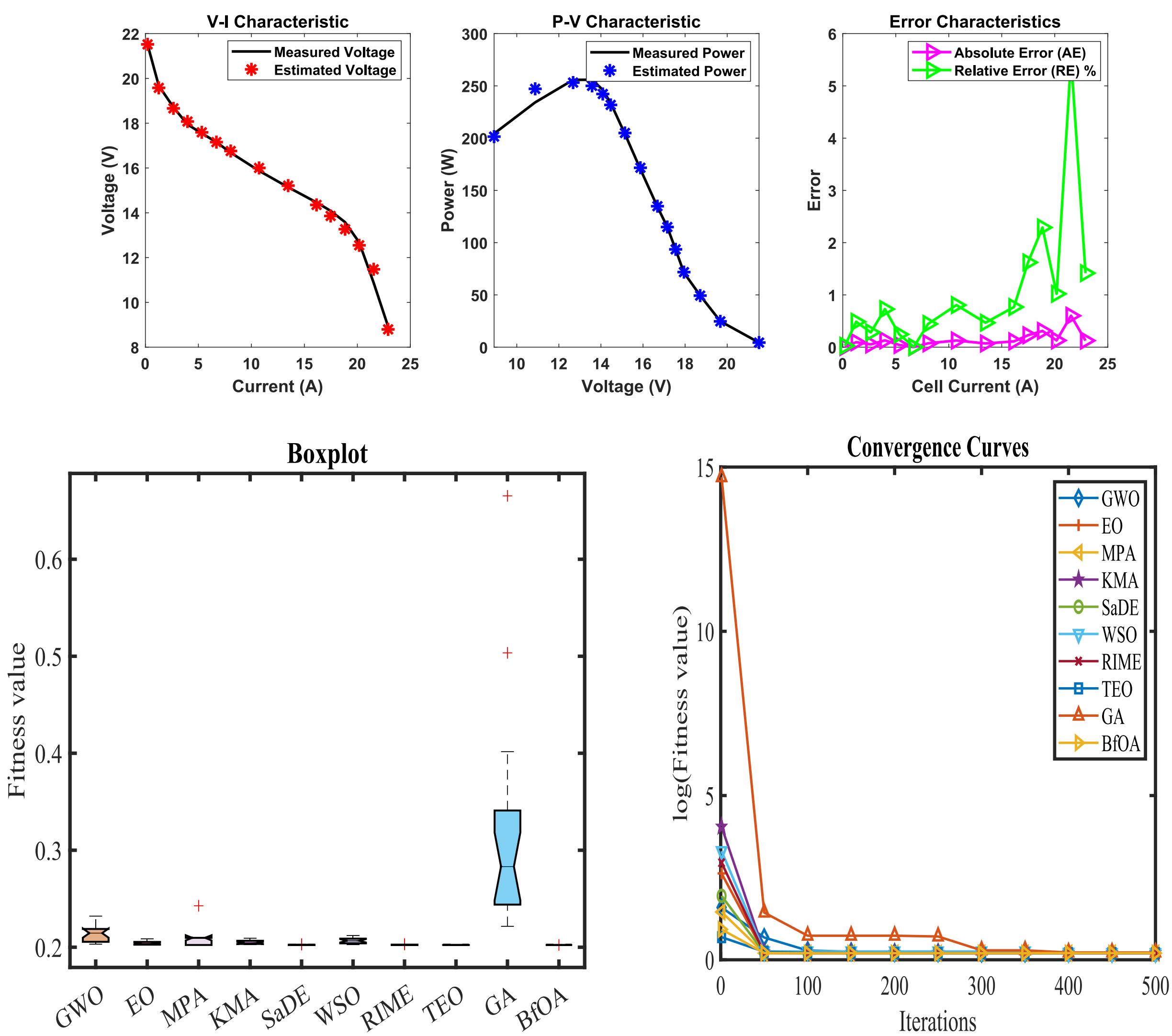

Fig. 10. Characteristic curves (a) P—V, V—I, and Error Curve, (b) Box-Plot (c) Convergence Curve for Sheet 9.

Table 21
Parameter Optimization and Function Maximization for Sheet 10.

Algorithm	GWO	EO	MPA	KMA	SaDE	WSO	RIME	TEO	GA	BfOA
ξ_1	−1.11704	−1.07876	−0.98827	−0.93209	−0.92675	−0.91202	−1.01056	−1.19664	−0.91345	−1.09226
ξ_2	0.002815	0.002813	0.003253	0.002975	0.002396	0.00239	0.002949	0.003409	0.002304	0.002744
ξ_3	3.61E-05	4.43E-05	0.000098	8.88E-05	4.53E-05	4.81E-05	6.96E-05	6.45E-05	4.12E-05	3.6E-05
ξ_4	−0.00014	−0.00014	−0.00014	−0.00014	−0.00014	−0.00014	−0.00014	−0.00014	−0.00014	−0.00014
λ	14	14	14	14	14	14	14	14.0015	14.4436	14
R_c	0.0008	0.0008	0.0008	0.000726	0.0008	0.000721	0.0008	0.000799	0.000549	0.0008
B	0.01518	0.015488	0.015503	0.015748	0.015502	0.015844	0.015625	0.015479	0.016134	0.015503
Min.	0.104686	0.104447	0.104446	0.104911	0.104446	0.105188	0.104497	0.104464	0.111599	0.104446
Max.	0.164661	0.126702	0.144677	0.113207	0.108637	0.118404	0.105004	0.104656	0.286334	0.104446
Mean	0.118975	0.109682	0.112964	0.109422	0.104713	0.111604	0.104673	0.104509	0.160156	0.104446
Std.	0.015161	0.005683	0.011682	0.003179	0.000952	0.003591	0.000123	5.01E-05	0.048221	3.29E-15
RT	8.361563	8.828214	7.699642	8.350757	16.46013	9.329824	8.998134	10.91276	16.96657	0.383702
FR	7.947368	6.263158	5.789474	6.789474	2.947368	7.263158	4.210526	3.263158	9.473684	1.052632

Table 22
Performance metrics of the Proposed algorithm for Sheet 10.

Vcell	Icell	Vest	AE	Pest	Pref	MBE	RE %
23.541	0.2729	23.47401	0.066992	6.406057	6.424339	0.000299	0.284575
21.4756	1.279	21.55584	0.080244	27.56992	27.46729	0.000429	0.37365
20.3484	2.6603	20.53214	0.183743	54.62166	54.13285	0.002251	0.902983
19.8969	3.9734	19.89719	0.00029	79.05949	79.05834	5.6E-09	0.001457
19.4642	5.3547	19.36757	0.09663	103.7075	104.225	0.000622	0.496449
19.0127	6.719	18.91714	0.09556	127.1043	127.7463	0.000609	0.502611
18.5049	8.0321	18.52373	0.018835	148.7845	148.6332	2.36E-05	0.101782
17.8835	10.7265	17.78336	0.100136	190.7532	191.8274	0.000668	0.559937
17.2808	13.472	17.06738	0.213425	229.9317	232.8069	0.003037	1.235039
16.2089	16.1664	16.3588	0.149896	264.4628	262.0396	0.001498	0.924778
15.8701	17.4966	15.99328	0.123182	279.8281	277.6728	0.001012	0.77619
15.5312	18.8608	15.59617	0.064966	294.1562	292.9309	0.000281	0.418293
15.1923	20.191	15.17005	0.022249	306.2985	306.7477	3.3E-05	0.146447
14.6282	21.5553	14.64549	0.01729	315.6879	315.3152	1.99E-05	0.118199
13.745	22.9195	13.70155	0.043454	314.0326	315.0285	0.000126	0.316147
			0.085126			**0.000727**	**0.477236**

boxplot comparison of fitness values shows BfOA's tight clustering with no outliers and minimal spread, indicating superior stability and reliability compared to algorithms like GWO and GA, which exhibit greater variability. Finally, Fig. 13(c) shows BfOA's rapid convergence, stabilizing within the first 50 iterations, while MPA and KMA take longer. This smooth and efficient convergence demonstrates BfOA's ability to quickly and effectively minimize fitness values, a key advantage in optimization.

4.1. Discussion

Researchers analyzing twelve PEMFC case studies demonstrated the superiority of the BfOA algorithm over other metaheuristic methods for parameter optimization. BfOA exhibited greater computational efficiency, higher accuracy in polarization curve fitting, and faster overall performance. Across all cases, BfOA achieved significantly lower Minimum Sum of Squared Errors (SSE), indicating a better match between experimental and simulated data. Its stability and reliable convergence were confirmed by the negligible standard deviation observed across multiple runs. BfOA's computational speed consistently surpassed all other algorithms, a crucial advantage for real-time applications and complex calculations. Graphical analysis further validated these findings: Figure a showcases BfOA's accuracy with near-perfect curve matching; Figure b illustrates its robustness through narrow SSE value distributions; and Figure c highlights its rapid convergence. While Figure a shows increased error at high currents, this is attributed to known mass transport limitations within PEMFC technology, a recognized issue unrelated to BfOA's optimization capabilities. Despite these inherent limitations, BfOA's consistently superior performance establishes it as a highly effective tool for PEMFC parameter optimization, offering significant advantages over existing methods. This makes BfOA a promising solution for real-world energy applications such as electric vehicles, renewable energy systems, and distributed power generation. Future work will investigate BfOA's performance with more complex fuel cell models and other energy systems to broaden its applicability.

5. Conclusion

Accurate parameter estimation is essential for the effective modeling, design, and control of complex fuel cell systems. Analyzing voltage-current (V—I) and power-voltage (P—V) characteristics, which vary with operating conditions, provides crucial information for this process. This study investigates twelve distinct fuel cell systems, employing a algorithm (BfOA) for parameter identification. The performance of BfOA is evaluated by comparing it against established optimization techniques.

- BfOA's tuning of the seven key fuel cell model parameters results in significantly improved prediction accuracy, closely aligning with real-world data across diverse operating conditions.
- Beyond minimizing the Sum of Squared Errors (SSE), BfOA significantly enhances accuracy across multiple error metrics, including

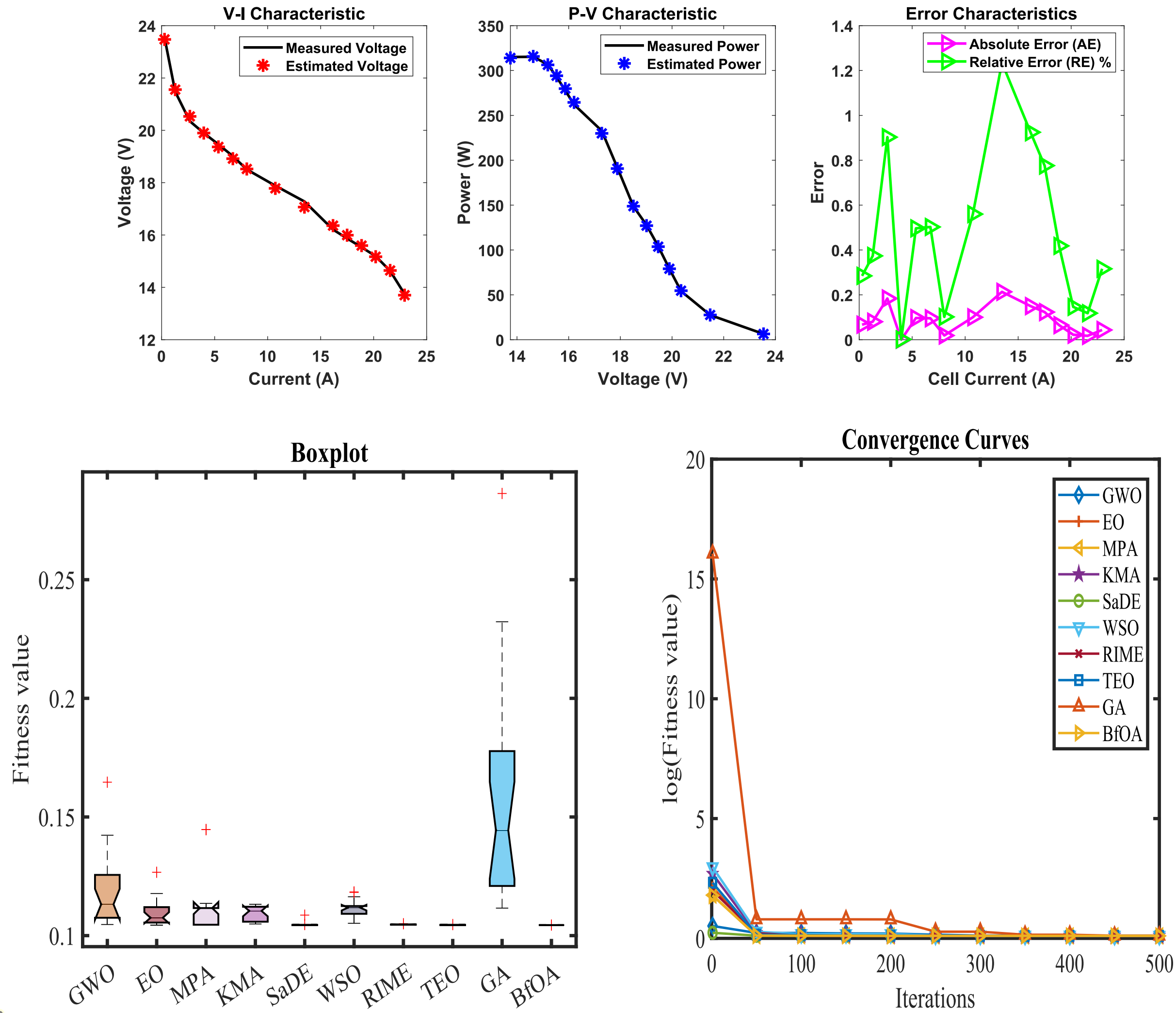

Fig. 11. Characteristic curves (a) P—V, V—I, and Error Curve, (b) Box-Plot (c) Convergence Curve for Sheet 10.

Table 23
Parameter Optimization and Function Maximization for Sheet 11.

Algorithm	GWO	EO	MPA	KMA	SaDE	WSO	RIME	TEO	GA	BfOA
ξ_1	−1.15769	−0.8532	−1.19969	−0.85589	−1.00454	−1.19898	−1.16503	−1.12652	−1.19969	−0.87999
ξ_2	0.002677	0.001567	0.002715	0.001858	0.002371	0.00278	0.003313	0.002823	0.00308	0.00168
ξ_3	4.34E-05	3.6E-05	0.000036	5.63E-05	5.79E-05	4.08E-05	8.76E-05	6.14E-05	6.26E-05	3.77E-05
ξ_4	−9.5E-05	−9.5E-05	−9.5E-05	−9.5E-05	−9.5E-05	−9.5E-05	−9.5E-05	−9.5E-05	−9.5E-05	−9.5E-05
λ	23	23	23	21.21822	23	22.00575	23	22.99929	14	23
R_c	0.0001	0.0001	0.0001	0.000143	0.0001	0.000134	0.0001	0.0001	0.000431	0.0001
B	0.034753	0.034812	0.034812	0.03456	0.034812	0.034906	0.034809	0.034851	0.029934	0.034812
Min.	0.075485	0.075484	0.075484	0.075581	0.075484	0.075561	0.075484	0.075485	0.078057	0.075484
Max.	0.090069	0.075753	0.076392	0.076013	0.075843	0.076285	0.07549	0.075506	0.117267	0.076103
Mean	0.081158	0.07558	0.075701	0.075777	0.075581	0.075856	0.075485	0.075489	0.099695	0.075615
Std.	0.005014	8.79E-05	0.000283	0.000138	0.000112	0.000183	1.4E-06	5.29E-06	0.012161	0.000259
RT	8.834201	9.18711	7.87367	8.55728	16.88026	9.478379	9.083234	10.97621	17.43251	0.343401
FR	8.263158	5.105263	4.315789	6.578947	4.842105	7.263158	2.526316	3.631579	9.894737	2.578947

Table 24
Performance metrics of the Proposed algorithm for Sheet 11.

Vcell	Icell	Vest	AE	Pest	Pref	MBE	RE %
9.53	0.104	9.707991	0.177991	1.009631	0.99112	0.002112	1.867695
9.38	0.199	9.438401	0.058401	1.878242	1.86662	0.000227	0.62261
9.2	0.307	9.244289	0.044289	2.837997	2.8244	0.000131	0.481397
9.24	0.403	9.112618	0.127382	3.672385	3.72372	0.001082	1.378594
9.1	0.511	8.988223	0.111777	4.592982	4.6501	0.000833	1.228322
8.94	0.614	8.883388	0.056612	5.4544	5.48916	0.000214	0.63324
8.84	0.704	8.798598	0.041402	6.194213	6.22336	0.000114	0.468344
8.75	0.806	8.707211	0.042789	7.018012	7.0525	0.000122	0.48902
8.66	0.908	8.618539	0.041461	7.825634	7.86328	0.000115	0.478761
8.45	1.075	8.474217	0.024217	9.109783	9.08375	3.91E-05	0.28659
8.41	1.126	8.429356	0.019356	9.491455	9.46966	2.5E-05	0.23016
8.2	1.28	8.28806	0.08806	10.60872	10.496	0.000517	1.073907
8.14	1.39	8.178149	0.038149	11.36763	11.3146	9.7E-05	0.468666
8.11	1.45	8.11327	0.00327	11.76424	11.7595	7.13E-07	0.040322
8	1.57	7.967689	0.032311	12.50927	12.56	6.96E-05	0.403891
			0.060498			**0.00038**	**0.676768**

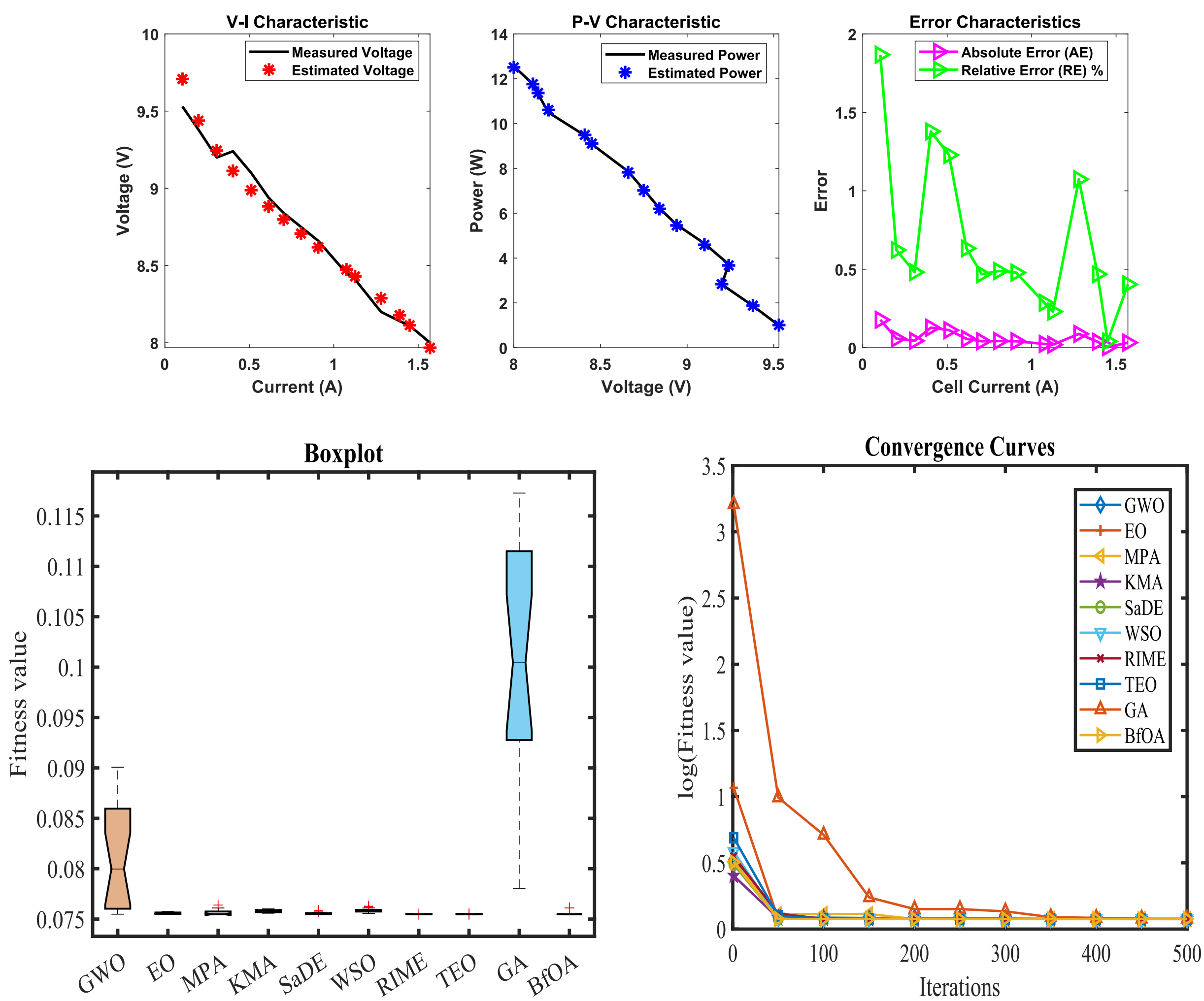

Fig. 12. Characteristic curves (a) P—V, V—I, and Error Curve, (b) Box-Plot (c) Convergence Curve for Sheet 11.

Table 25
Parameter Optimization and Function Maximization for Sheet 12.

Algorithm	GWO	EO	MPA	KMA	SaDE	WSO	RIME	TEO	GA	BfOA
ξ_1	−0.85348	−0.8532	−1.19969	−0.94376	−0.87878	−0.88795	−0.98553	−1.11844	−0.89588	−0.8532
ξ_2	0.001616	0.001839	0.002981	0.00225	0.002219	0.001762	0.00267	0.0032	0.002346	0.002475
ξ_3	3.6E-05	5.22E-05	5.44E-05	6.09E-05	7.37E-05	3.86E-05	8.15E-05	8.9E-05	7.87E-05	9.8E-05
ξ_4	−9.5E-05	−9.5E-05	−9.5E-05	−9.5E-05	−9.5E-05	−9.5E-05	−9.5E-05	−9.5E-05	−9.5E-05	−9.5E-05
λ	14.37389	14	14	14	14.00164	14.15766	14	14.07342	22.15695	14
R_c	0.000535	0.000798	0.0008	0.000412	0.000734	0.000185	0.0008	0.000741	0.000397	0.0008
B	0.04925	0.048486	0.048483	0.049095	0.048565	0.049421	0.048462	0.048565	0.052486	0.048483
Min.	0.064213	0.064194	0.064194	0.064201	0.064196	0.064205	0.064194	0.064195	0.064855	0.064194
Max.	0.103778	0.064237	0.107	0.064278	0.064288	0.064409	0.064199	0.064218	0.121303	0.064194
Mean	0.071575	0.064203	0.070516	0.064233	0.06423	0.064264	0.064196	0.064201	0.080342	0.064194
Std.	0.01216	1.19E-05	0.01493	2.02E-05	2.48E-05	5.47E-05	1.51E-06	6.41E-06	0.015849	1.31E-16
RT	8.630206	8.793425	7.586806	8.243002	16.48885	9.244015	8.723668	10.92477	16.95799	0.358489
FR	8.736842	3.736842	6.894737	5.947368	5.631579	7.105263	2.368421	3.947368	9.631579	1

Table 26
Performance metrics of the Proposed algorithm for Sheet 12.

Vest	Vcell	Icell	AE	Pest	Pref	MBE	RE %
9.999676	9.87	0.097	0.129676	0.969969	0.95739	0.001121	1.313835
9.926757	9.84	0.115	0.086757	1.141577	1.1316	0.000502	0.881673
9.767163	9.77	0.165	0.002837	1.611582	1.61205	5.37E-07	0.02904
9.669211	9.7	0.204	0.030789	1.972519	1.9788	6.32E-05	0.317416
9.573412	9.61	0.249	0.036588	2.38378	2.39289	8.92E-05	0.380725
9.527679	9.59	0.273	0.062321	2.601056	2.61807	0.000259	0.649859
9.436217	9.5	0.326	0.063783	3.076207	3.097	0.000271	0.671399
9.329837	9.4	0.396	0.070163	3.694616	3.7224	0.000328	0.746413
9.191099	9.26	0.5	0.068901	4.595549	4.63	0.000316	0.744073
9.046907	9.05	0.621	0.003093	5.618129	5.62005	6.38E-07	0.034173
8.946522	8.93	0.711	0.016522	6.360977	6.34923	1.82E-05	0.185017
8.853561	8.83	0.797	0.023561	7.056288	7.03751	3.7E-05	0.266829
8.63028	8.54	1.006	0.09028	8.682062	8.59124	0.000543	1.057145
8.481146	8.42	1.141	0.061146	9.676988	9.60722	0.000249	0.726203
8.200534	8.27	1.37	0.069466	11.23473	11.3299	0.000322	0.839981
			0.054392			**0.000275**	**0.589585**

Absolute Error (AE), Relative Error (RE), and Mean Bias Error (MBE). Consistently outperforming other algorithms, BfOA demonstrates superior accuracy and reliability by minimizing these metrics across all tested cases.

- Using BfOA-optimized parameters, the fuel cell model accurately predicts performance, evidenced by the strong correlation between predicted and measured current-voltage (I/V) and power-voltage (P/V) curves.

These results position BfOA as a highly effective method for integration within electronic component simulators, facilitating accurate analysis and study of PEMFC devices. Its precision, robustness, and computational efficiency make BfOA a promising tool for PEMFC modeling and simulation.

5.1. Future work

Future research will explore BfOA's applicability to diverse fuel cell technologies, including solid oxide fuel cells (SOFCs), to assess its robustness and generalizability. Integrating real-time data and dynamic environmental factors into parameter estimation will improve its adaptability to real-world operation. BfOA with machine learning may enable predictive degradation modeling and optimized lifetime performance strategies. Finally, embedding BfOA within systems will facilitate real-time PEMFC control and monitoring, enabling efficient, automated fuel cell management in practical applications.While extensive simulations across twelve commercial PEMFC systems validated the BfOA-optimized parameters, demonstrating superior I-V and P—V curve prediction accuracy compared to other algorithms, hardware-based testing on real PEMFC systems is still pending. Acknowledging this limitation, future research will focus on experimental validation to confirm BfOA's real-world applicability. This will involve implementing the optimized parameters in physical PEMFC systems and evaluating their performance under various operating conditions. This crucial step will bridge the gap between simulation and practice, ensuring the algorithm's predictions translate effectively to real-world fuel cell operation. This validation process will also provide valuable insights into any discrepancies, leading to further improvements in the algorithm's accuracy and reliability in practical applications.

CRediT authorship contribution statement

Manish Kumar Singla: Writing – original draft, Validation, Software. **S.A. Muhammed Ali:** Writing – review & editing, Supervision. **Jyoti Gupta:** Validation, Formal analysis, Data curation, Conceptualization. **Pradeep Jangir:** Resources, Methodology, Investigation. **Arpita:** Writing – original draft, Validation, Supervision. **Ramesh Kumar:** Visualization, Validation, Supervision. **Reena Jangid:** Writing – review & editing, Validation. **Mohammad Khishe:** Writing – review & editing, Supervision, Software, Investigation.

Informed consent statement

Not applicable.

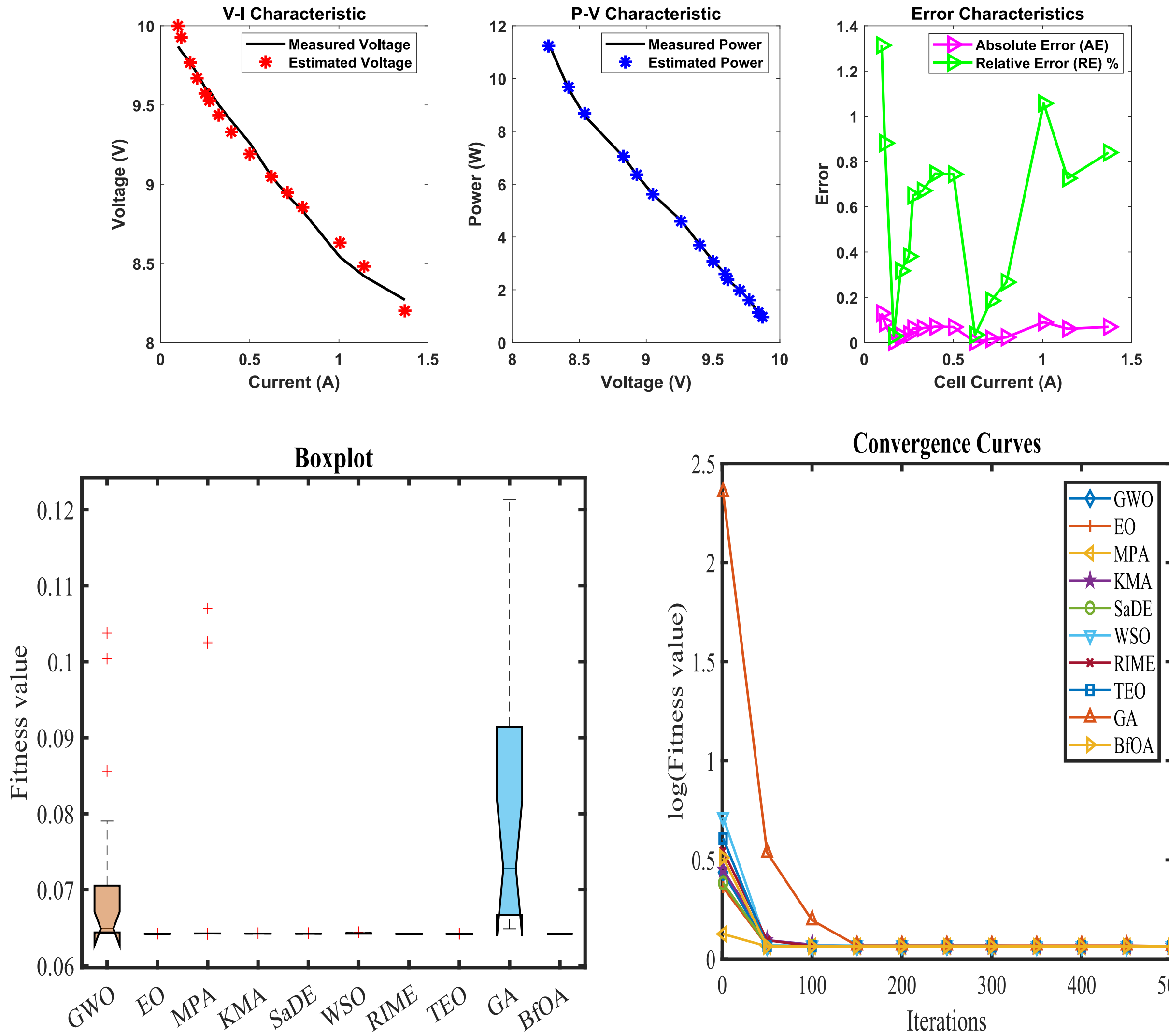

Fig. 13. Characteristic curves (a) P—V, V—I, and Error Curve, (b) Box-Plot (c) Convergence Curve for Sheet 12.

Institutional review board statement

Not applicable.

Funding

No Funding.

Declaration of competing interest

The authors declare that they have no known competing financial interests or personal relationships that could have appeared to influence the work reported in this paper.

Acknowledgment

The authors would like to acknowledge the funding from the Ministry of Higher Education Malaysia, through a Fundamental Research Grant Scheme (FRGS) with code FRGS/1/2023/TK08/UKM/02/5.

Appendix A. Supplementary data

Supplementary data to this article can be found online at https://doi.org/10.1016/j.elecom.2025.108033.

Data availability

The data presented in this study are available through email upon request to the corresponding author.

References

[1] A.Z. Kouache, A. Djafour, M.B. Danoune, K.M.S. Benzaoui, A. Gougui, Accurate key parameters estimation of PEM fuel cells using self-adaptive bonobo optimizer, Comput. Chem. Eng. 192 (2025) 108894.
[2] A.A. El-Fergany, A.M. Agwa, Red-billed blue magpie optimizer for electrical characterization of fuel cells with prioritizing estimated parameters, Technologies 12 (9) (2024) 156.
[3] S. Saidi, S. Marrouchi, B.N. Alhasnawi, P.K. Pathak, O. Alshammari, A. Albaker, R. Abbassi, Precise parameter identification of a PEMFC model using a robust enhanced salp swarm algorithm, Int. J. Hydrog. Energy 71 (2024) 937–951.
[4] M.H. Elfar, M. Fawzi, A.S. Serry, M. Elsakka, M. Elgamal, A. Refaat, Optimal parameters identification for PEMFC using autonomous groups particle swarm optimization algorithm, Int. J. Hydrog. Energy 69 (2024) 1113–1128.
[5] B. Yang, B. Liang, Y. Qian, R. Zheng, S. Su, Z. Guo, L. Jiang, Parameter identification of PEMFC via feedforward neural network-pelican optimization algorithm, Appl. Energy 361 (2024) 122857.
[6] A.M. Shaheen, A. Alassaf, I. Alsaleh, A.A. El-Fergany, Enhancing model characterization of PEM fuel cells with human memory optimizer including sensitivity and uncertainty analysis, Ain Shams Eng. J. 15 (11) (2024) 103026.
[7] H.M. Sultan, A.S. Menesy, A. Korashy, A.G. Hussien, S. Kamel, Enhancing parameter identification for proton exchange membrane fuel cell using modified manta ray foraging optimization, Energy Rep. 12 (2024) 1987–2013.
[8] E.H. Houssein, N.A. Samee, M. Alabdulhafith, M. Said, Extraction of PEM fuel cell parameters using walrus optimizer, AIMS Mathematics 9 (5) (2024) 12726–12750.

[9] K. Priya, V. Selvaraj, N. Ramachandra, N. Rajasekar, Modelling of PEM fuel cell for parameter estimation utilizing clan co-operative based spotted hyena optimizer, Energy Convers. Manag. 309 (2024) 118371.
[10] H. Ashraf, A. Draz, A comprehensive survey of artificial intelligence-based techniques for performance enhancement of solid oxide fuel cells: test cases with debates, Artif. Intell. Rev. 57 (2) (2024) 29.
[11] B. Zhang, R. Wang, D. Jiang, Y. Wang, J. Wang, B. Ruan, Parameter identification of proton exchange membrane fuel cell based on swarm intelligence algorithm, Energy 283 (2023) 128935.
[12] S.M. Ebrahimi, S. Hasanzadeh, S. Khatibi, Parameter identification of fuel cell using repairable grey wolf optimization algorithm, Appl. Soft Comput. 147 (2023) 110791.
[13] F. Duan, C. Chen, F. Song, S. Zhang, X. Li, M. Eslami, An optimal parameters estimation for the proton exchange membrane fuel cells based on amended deer hunting optimization algorithm, Sustain Energy Technol Assess 58 (2023) 103364.
[14] P. He, X. Zhou, M. Liu, K. Xu, X. Meng, B. Yang, Generalized regression neural network based Meta-heuristic algorithms for parameter identification of proton exchange membrane fuel cell, Energies 16 (14) (2023) 5290.
[15] A. Rubio, W. Agila, L. González, J. Aviles-Cedeno, Distributed intelligence in autonomous PEM fuel cell control, Energies 16 (12) (2023) 4830.
[16] M.A. Ali, M.E. Mandour, M.E. Lotfy, Adaptive estimation of quasi-empirical proton exchange membrane fuel cell models based on coot bird optimizer and data accumulation, Sustainability 15 (11) (2023) 9017.
[17] M. Abdel-Basset, R. Mohamed, M. Abouhawwash, On the facile and accurate determination of the highly accurate recent methods to optimize the parameters of different fuel cells: simulations and analysis, Energy 272 (2023) 127083.
[18] F. Yang, X. Xu, Y. Li, D. Chen, S. Hu, Z. He, Y. Du, A review on mass transfer in multiscale porous media in proton exchange membrane fuel cells: mechanism, modeling, and parameter identification, Energies 16 (8) (2023) 3547.
[19] Z. Guo, Z. Ye, P. Ni, C. Cao, X. Wei, J. Zhao, X. He, Intelligent digital twin modelling for hybrid PV-SOFC power generation system, Energies 16 (6) (2023) 2806.
[20] U. Mitra, A. Arya, S. Gupta, A comprehensive and comparative review on parameter estimation methods for modelling proton exchange membrane fuel cell, Fuel 335 (2023) 127080.
[21] Liu, D., Yang, X., Guan, C., Qi, T., & Zheng, Q. (2023). A new method of parameter identification for proton exchange membrane fuel cell based on hybrid particle swarm optimization with differential evolution algorithm. Therm. Sci., (00), 62-62.
[22] M. Abdel-Basset, R. Mohamed, L. Abdel-Fatah, M. Sharawi, K.M. Sallam, Improved metaheuristic algorithms for optimal parameters selection of proton exchange membrane fuel cells: a comparative study, IEEE Access 11 (2023) 7369–7397.
[23] T. Wang, H. Huang, X. Li, X. Guo, M. Liu, H. Lei, Optimal estimation of proton exchange membrane fuel cell model parameters based on an improved chicken swarm optimization algorithm, Int. J. Green Energy 20 (9) (2023) 946–965.
[24] H. Rezk, T. Wilberforce, A.G. Olabi, R.M. Ghoniem, E.T. Sayed, M. Ali Abdelkareem, Optimal parameter identification of a PEM fuel cell using recent optimization algorithms, Energies 16 (14) (2023) 5246.
[25] J. Zhou, M.A. Ali, K. Sharma, A.A. Alizadeh, S.F. Almojil, A.I. Almohana, B. F. Ibrahim, Improved fish migration optimization method to identify PEMFC parameters, Int. J. Hydrog. Energy 48 (52) (2023) 20028–20040.
[26] M.S. Shalaby, M.S. Mansour, A.B. Eldin, H. Abdallah, I.I. Ibrahim, M. Abdel Fattah, G. Sołowski, Removal of phenol from sour water by poly (vinyl alcohol)/polyamide-reverse osmosis membranes, Chem. Eng. Technol. 45 (12) (2022) 2130–2138.
[27] T. Wilberforce, M. Biswas, A study into proton exchange membrane fuel cell power and voltage prediction using artificial neural network, Energy Rep. 8 (2022) 12843–12852.
[28] J. Li, T. Qian, T. Yu, Data-driven coordinated control method for multiple systems in proton exchange membrane fuel cells using deep reinforcement learning, Energy Rep. 8 (2022) 290–311.
[29] M. Rezaie, E. Akbari, N. Ghadimi, N. Razmjooy, M. Ghadamyari, Model parameters estimation of the proton exchange membrane fuel cell by a modified golden jackal optimization, Sustain Energy Technol Assess 53 (2022) 102657.
[30] R. Ding, S. Zhang, Y. Chen, Z. Rui, K. Hua, Y. Wu, J. Liu, Application of machine learning in optimizing proton exchange membrane fuel cells: a review, Energy and AI 9 (2022) 100170.
[31] B. Yang, D. Li, C. Zeng, Y. Han, J. Li, Bald eagle search algorithm for parameter identification of proton exchange membrane fuel cell, Front. Energy Res. 10 (2022) 885461.
[32] R. Losantos, M. Montiel, R. Mustata, F. Zorrilla, L. Valino, Parameter characterization of HTPEMFC using numerical simulation and genetic algorithms, Int. J. Hydrog. Energy 47 (7) (2022) 4814–4826.
[33] Y. Liao, Educational evaluation of piano performance by the deep learning neural network model, Mob. Inf. Syst. 2022 (1) (2022) 6975824.
[34] J. Li, J. Geng, T. Yu, Multi-objective optimal control for proton exchange membrane fuel cell via large-scale deep reinforcement learning, Energy Rep. 7 (2021) 6422–6437.
[35] M. Abdel-Basset, R. Mohamed, V. Chang, An efficient parameter estimation algorithm for proton exchange membrane fuel cells, Energies 14 (21) (2021) 7115.
[36] J. Li, Y. Li, T. Yu, Control method for PEMFC using improved deep deterministic policy gradient algorithm, Front. Energy Res. 9 (2021) 753064.
[37] E.A. Gouda, M.F. Kotb, A.A. El-Fergany, Jellyfish search algorithm for extracting unknown parameters of PEM fuel cell models: steady-state performance and analysis, Energy 221 (2021) 119836.
[38] Y. Zhu, N. Yousefi, Optimal parameter identification of PEMFC stacks using adaptive sparrow search algorithm, Int. J. Hydrog. Energy 46 (14) (2021) 9541–9552.
[39] M. Alizadeh, F. Torabi, Precise PEM fuel cell parameter extraction based on a self-consistent model and SCCSA optimization algorithm, Energy Convers. Manag. 229 (2021) 113777.
[40] D. Setiawan, S. Suyanto, B. Erfianto, A.A. Gozali, Battlefield optimization algorithm, Expert Syst. Appl. 266 (2025) 126097.
[41] H.M. Sultan, A.S. Menesy, M.S. Hassan, F. Jurado, S. Kamel, Standard and quasi oppositional bonobo optimizers for parameter extraction of PEM fuel cell stacks, Fuel 340 (2023) 127586.
[42] A.S. Menesy, H.M. Sultan, A. Selim, M.G. Ashmawy, S. Kamel, Developing and applying chaotic Harris hawks optimization technique for extracting parameters of several proton exchange membrane fuel cell stacks, IEEE Access 8 (2019) 1146–1159.
[43] Y. Chen, G. Zhang, New parameters identification of proton exchange membrane fuel cell stacks based on an improved version of African vulture optimization algorithm, Energy Rep. 8 (2022) 3030–3040.
[44] H.M. Hasanien, M.A. Shaheen, R.A. Turky, M.H. Qais, S. Alghuwainem, S. Kamel, F. Jurado, Precise modeling of PEM fuel cell using a novel enhanced transient search optimization algorithm, Energy 247 (2022) 123530.
[45] R. Shan, T. Rezaei, Lung cancer diagnosis based on an ann optimized by improved Teo algorithm, Comput. Intell. Neurosci. 2021 (1) (2021) 6078524.
[46] H. Rezaei, O. Bozorg-Haddad, X. Chu, Grey wolf optimization (GWO) algorithm, Advanced optimization by nature-inspired algorithms (2018) 81–91.
[47] H. Su, D. Zhao, A.A. Heidari, L. Liu, X. Zhang, M. Mafarja, H. Chen, RIME: a physics-based optimization, Neurocomputing 532 (2023) 183–214.
[48] A. Faramarzi, M. Heidarinejad, B. Stephens, S. Mirjalili, Equilibrium optimizer: a novel optimization algorithm, Knowl.-Based Syst. 191 (2020) 105190.
[49] A. Faramarzi, M. Heidarinejad, S. Mirjalili, A.H. Gandomi, Marine predators algorithm: a nature-inspired metaheuristic, Expert Syst. Appl. 152 (2020) 113377.
[50] S. Suyanto, A.A. Ariyanto, A.F. Ariyanto, Komodo mlipir algorithm, Appl. Soft Comput. 114 (2022) 108043.
[51] A.K. Qin, P.N. Suganthan, Self-adaptive differential evolution algorithm for numerical optimization, in: In 2005 IEEE Congress on Evolutionary Computation vol. 2, IEEE, 2005, September, pp. 1785–1791.
[52] M. Braik, A. Hammouri, J. Atwan, M.A. Al-Betar, M.A. Awadallah, White shark optimizer: a novel bio-inspired meta-heuristic algorithm for global optimization problems, Knowl.-Based Syst. 243 (2022) 108457.
[53] Mirjalili, S., & Mirjalili, S. 2019. Genetic algorithm. Evolutionary algorithms and neural networks: theory and applications, 43–55.
[54] A. Rowe, X. Li, Mathematical modeling of proton exchange membrane fuel cells, J. Power Sources 102 (1–2) (2001) 82–96.
[55] J.M. Corrêa, F.A. Farret, L.N. Canha, M.G. Simoes, An electrochemical-based fuel-cell model suitable for electrical engineering automation approach, IEEE Trans. Ind. Electron. 51 (5) (2004) 1103–1112.
[56] F.Z. Aouali, M. Becherif, H.S. Ramadan, M. Emziane, A. Khellaf, K. Mohammedi, Analytical modelling and experimental validation of proton exchange membrane electrolyser for hydrogen production, Int. J. Hydrog. Energy 42 (2) (2017) 1366–1374.
[57] J.C. Amphlett, R.M. Baumert, R.F. Mann, B.A. Peppley, P.R. Roberge, T.J. Harris, Performance modeling of the Ballard mark IV solid polymer electrolyte fuel cell: I. Mechanistic model development, J. Electrochem. Soc. 142 (1) (1995) 1.
[58] R.F. Mann, J.C. Amphlett, M.A. Hooper, H.M. Jensen, B.A. Peppley, P.R. Roberge, Development and application of a generalised steady-state electrochemical model for a PEM fuel cell, J. Power Sources 86 (1–2) (2000) 173–180.
[59] J.C. Amphlett, R.M. Baumert, R.F. Mann, B.A. Peppley, P.R. Roberge, T.J. Harris, Performance modeling of the Ballard mark IV solid polymer electrolyte fuel cell: II. Empirical model development, J. Electrochem. Soc. 142 (1) (1995) 9.
[60] Z.J. Mo, X.J. Zhu, L.Y. Wei, G.Y. Cao, Parameter optimization for a PEMFC model with a hybrid genetic algorithm, Int. J. Energy Res. 30 (8) (2006) 585–597.
[61] B. Alatas, Chaotic harmony search algorithms, Appl. Math. Comput. 216 (9) (2010) 2687–2699.
[62] T.V. Nguyen, R.E. White, A water and heat management model for proton-exchange-membrane fuel cells, J. Electrochem. Soc. 140 (8) (1993) 2178.
[63] A.A. El-Fergany, Electrical characterisation of proton exchange membrane fuel cells stack using grasshopper optimiser, IET Renewable Power Generation 12 (1) (2018) 9–17.
[64] M. Ali, M.A. El-Hameed, M.A. Farahat, Effective parameters' identification for polymer electrolyte membrane fuel cell models using grey wolf optimizer, Renew. Energy 111 (2017) 455–462.
[65] S. Tzu, Sun Tzu Art of War, Vij Books India Pvt Ltd., 2012.
[66] D.J. Mrozek, Air Power and the Ground War in Vietnam, The Minerva Group, Inc., 2002.
[67] W.F. Owen, On tactics: a theory of victory in battle, Parameters 47 (4) (2017) 125–126.
[68] A.A. Mughal, The art of cybersecurity: defense in depth strategy for robust protection, Int. J. Intelligent Automation Comput. 1 (1) (2018) 1–20.
[69] A. Atmowiloto, Senopati pamungkas 1, Gramedia Pustaka Utama, 2003.

[70] L.K. Hariadi, Gajah Mada: Bergelut dalam kemelut takhta dan angkara 2, Tiga Serangkai, 2008.
[71] A. Susilo, Sejarah perjuangan jenderal soedirman dalam mempertahankan indonesia (1945-1950), HISTORIA: Jurnal Program Studi Pendidikan Sejarah 6 (1) (2018) 57–68.
[72] J.W. Lee, Warfare in the classical age, in: A companion to the Classical Greek world, 2006, pp. 480–508.
[73] M. Song, H. Jia, L. Abualigah, Q. Liu, Z. Lin, D. Wu, M. Altalhi, Modified Harris hawks optimization algorithm with exploration factor and random walk strategy, Comput. Intell. Neurosci. 2022 (1) (2022) 4673665.
[74] B.S. Yıldız, S. Kumar, N. Pholdee, S. Bureerat, S.M. Sait, A.R. Yildiz, A new chaotic Lévy flight distribution optimization algorithm for solving constrained engineering problems, Expert. Syst. 39 (8) (2022) e12992.
[75] Z. Liu, S. Huang, Carbon option price forecasting based on modified fractional Brownian motion optimized by GARCH model in carbon emission trading, North Am. J. Economics Finance 55 (2021) 101307.
[76] D. Bohrer, America's Special Forces, Zenith Imprint, 1998.
[77] C. Pfarrer, SEAL Target Geronimo: The Inside Story of the Mission to Kill Osama bin Laden, St. Martin's Press, 2011.